Acta Universitatis Carolinae. Mathematica et Physica

R. Král; Pavel Lukáč

Mechanisms of plastic deformation in Al-Mg and Al-Zn-Mg alloys

Acta Universitatis Carolinae. Mathematica et Physica, Vol. 39 (1998), No. 1-2, 49--90

Persistent URL: http://dml.cz/dmlcz/142689

Mechanisms of Plastic Deformation in Al-Mg and Al-Zn-Mg Alloys

R. KRÁL and P. LUKÁČ

Praha*)

Received 10. February 1998

Deformation behaviour of two pure aluminium-magnesium alloys with actual weight concentrations of 2.6% Mg and 4.8% Mg, respectively, and a commercial aluminium alloy of type 7020 with 5 wt.% Zn and 1.2 wt.% Mg was investigated in the temperature range 193—523 K. Tensile tests with constant cross-head speed were performed for initial strain rates from the interval $6.6 \times 10^{-7}\,\mathrm{s}^{-1} \leq \dot{\varepsilon}_0 \leq 2.4 \times 10^{-2}\,\mathrm{s}^{-1}$.

Experimental work hardening curves are compared with the predictions of theoretical models proposed in the literature. Among them the models proposed by Malygin and lately by Lukáč and Balík were found to be applicable in the whole temperature range for all strain rates: The shape of the work hardening behaviour is described satisfactory in both models. The description by the Lukáč and Balík model is better in the case of Al-Zn-Mg alloy where also the stage IV of deformation is reached. The parameters of the models, which were obtained from the fits of experimental data and which have connection to various microstructural processes, are compared with the theoretical predictions. The role of various hardening and softening processes at different temperatures is considered. Parameter values were found to be in good agreement with theoretical values, observed microstructure (TEM) and measured dislocation density (XPA).

In the samples deformed at suitable strain rates and/or temperatures the Portevin–Le Châtelier (PLC) effect (serrated flow) was observed. The critical strains for the onset and termination of PLC effect have been measured as a function of strain rate and temperature. Experimental data are compared with the analytical model developed by Kubin and Estrin using an adoption of the model proposed by Balík and Lukáč. The model predictions of the strain rate dependence of the critical strain for the onset of the PLC effect are found to be in a good qualitative agreement with the experimental data in a limited range of strain rates corresponding to critical strains about 2% or higher in the case of the Al–4.8%Mg alloy and about 0.8% and higher in the case of Al–2.6%Mg alloy. For lower critical strains the model exhibits systematic deviations from experimental data. On the basis of a known work hardening behaviour of the investigated alloy a possible modification of the evolution equations of the mobile and immobile dislocations which are used in the model of Kubin and Estrin is suggested.

1. Introduction

The flow stress of crystalline materials σ depends on the dislocation structure which may be represented by the average dislocation density ϱ for which holds

*) Department of Metal Physics, Charles University, Ke Karlovu 5, CZ-12116 Praha 2, Czech Republic

$\sigma \propto \sqrt{\varrho}$. The dislocation structure can change during deformation (tensile test). A part of mobile dislocations is stored, forms consequently new obstacles for dislocation motion and contributes in this way to hardening. On the other hand, dislocations may annihilate or rearrange to form sub-boundaries of relatively low energy, which contributes to softening (recovery). A strong decrease in the work hardening rate Θ

$$\Theta = \left(\frac{\partial \sigma}{\partial \varepsilon}\right)_{\dot{\varepsilon},T} \tag{1}$$

(where ε is the true plastic strain and T is temperature) with increasing stress σ is caused by dynamic recovery due to cross-slip and/or climb of dislocations: Cross-slip of screw dislocations allows dislocations to overcome obstacles to their motion. Climb of edge dislocations depends on the presence of vacancies which can enable climb even at very low deformation temperatures [1]. Formulating an evolution equation for the dislocation density leads to a model equation which describes the stress dependence of the work hardening rate.

The processes of work hardening in crystalline matter have attracted the attention of numerous investigators over many decades, starting with the work of Taylor [2] who applied his new dislocation theory of plasticity to explain the work hardening behaviour in aluminium. In the last two decades a wide variety of models have been suggested to describe the work hardening in crystalline materials — see e.g. the works [3] to [16] — which are based on different microstructural mechanisms. Some of these models are designed merely for low temperature deformation and/or high temperature creep tests [12 – 15] and are thus irrelevant for the present work. The model of Argon and Haasen [16] suggests only a possible hardening mechanism concerning the late stages of work hardening and does not give a full description which could be apllied in the analysis of work hardening curves. The model of Zehetbauer [10, 11] was lately developed for the description of work hardening behaviour in cell-forming materials at stages IV and V, which are, however, only marginal in the present work.

In general, the model equation, which contains adjustable parameters, can be fitted to the experimental data (*i.e.* work hardening curves) and the values of model parameters (obtained from this fit) and their temperature and strain rate dependence, as well as the 'quality' of the fit, can help us, in the view of observed microstructure (by the means of TEM and light microscopy) of the samples and measured average dislocation density (X-ray Peak Profile Analysis, XPA), to judge on the validity of respective models. In our previous works we have analyzed work hardening curves in zirconium based alloys [17, 18, 19] and Al–5%Zn–1.%Mg alloy [20]. We have shown that the course of the whole $\Theta(\sigma)$ curve cannot be, in any of investigated alloys, described satisfactorily by the models of Kocks [3], Estrin and Mecking [4] or Roberts [5]. Therefore, in the following we will not be concerned with any of these models.

In the present work, the experimental data obtained for three aluminium based alloys deformed at various temperatures and strain rates are compared with the work hardening models proposed in the literature by Gottstein and Argon [6], Prinz and Argon [7], Malygin [8], and Lukáč and Balík [9]. The first aim is to make a decision on the relevance of these models [6] to [9] for the description of the work hardening behaviour in the present case.

In a certain range of temperatures and strain rates, many solid solutions exhibit the Portevin–Le Châtelier (PLC) effect, *i.e.* the appearance of instabilities (serrations and/or drops) on the stress-strain curve in the course of tensile testing. This instable behaviour often commences after a finite amount of plastic strain ε_c and in some cases can terminate at a larger value of strain ε_c^* again. The PLC effect has been investigated intensively in the past decades and a great deal of experimental data have been gathered, however the nature of the PLC effect has not yet been fully explained. It is commonly accepted that the PLC effect occurs in the region where the strain rate sensitivity (SRS) of the flow stress becomes negative (for details see *e.g.* [21] and references therein). A wide variety of models have been proposed [22–28].

It is generally assumed that the PLC effect arises from repeated locking and unlocking of mobile dislocations by diffusing solute atoms. In the theories based on the Cottrell model [22] it is supposed that the solute atmospheres are being formed on the mobile dislocations by bulk diffusion which is enhanced by the deformation induced vacancies. Both the vacancy concentration and mobile dislocation density are supposed to increase as a power of strain and contribute to the value of critical strain ε_c [23, 24]. Nevertheless, Kocks *et al.* [29] have shown that the vacancy concentration does not significantly affect the onset of jerky flow. In some other models [25, 26] the occurrence of PLC effect is explained without any effect of deformation induced vacancies being taken into account.

The model of Kubin and Estrin [27, 28] explains the critical strains for the occurrence of the PLC effect in terms of the strain dependence of the mobile and forest dislocation densities. It yields semi-quantitative results which can be compared with experimental data. Such comparison has been done by Balík and Lukáč [30] for the Al–2.84%Mg–0.40%Mn alloy (in the following will be referred to as Al–3%Mg) deformed at room temperature at various strain rates. A good qualitative agreement with the model predictions has been found, however only the fits which were performed for limited ranges of experimental data (and where the fit parameters were bounded by further conditions) yielded physically acceptable values of fit parameters. The second aim of this paper is to investigate the strain rate dependence of the critical strain for a pure Al–4.8%Mg alloy deformed at room temperature. The obtained experimental data will be compared with predictions of the model of Kubin and Estrin [27, 28]. Since the mechanisms of dislocation interaction, storage and recovery must be same in both cases, the comparison of fit parameters connected to work hardening behaviour and PLC effect, respectively, can help us to judge on the validity of the respective models.

2.1 Models for Work Hardening and Softening

In this section we will first give a short overview of the work hardening models of Kocks [3] and Estrin and Mecking [4] which we have tested in our previous works [17, 18] and then we will continue with a description of some more developed models proposed by Gottstein and Argon [6], Prinz and Argon [7], Malygin [8], and Lukáč and Balík [9].

Model of Kocks. Assuming that i) the mean free path of dislocations is proportional to the average dislocation spacing and ii) the change in the dislocation density is due to some recovery, Kocks [3] supposed the evolution equation in the form

$$\frac{\partial \varrho}{\partial \gamma} = \kappa_f \varrho^{1/2} - \frac{L_{CS}\varrho}{b} \tag{2}$$

where L_{CS} is the average length of the dislocation segment recovered in one recovery event (due to cross-slip), κ_f is a geometrical factor based on the assumption that the mean free path of dislocation glide is proportional to the average spacing between forest dislocations, γ is the plastic shear strain and b is the magnitude of the Burgers vector of dislocations. L_{CS} is a function of temperature and strain rate. He has obtained the stress dependence of the work hardening rate in the following form

$$\Theta = \Theta_0 \left(1 - \frac{\sigma}{\sigma_S}\right) \tag{3}$$

where $\Theta_0 = \alpha G b \kappa_f / 2$ and $\sigma_S = \alpha G b^2 \kappa_f / L_{CS}$, G is the shear modulus and α is a numerical constant. Equation (3) cannot obviously describe the whole work hardening curve which consists of two parts with significantly different slopes and which is common for many materials [17].

Model of Estrin and Mecking. In contrary to this, Estrin and Mecking [4] have assumed that the mean free path of dislocations is constant and it is determined by the spacing between impenetrable obstacles. Finally they obtained

$$\frac{\partial \varrho}{\delta \gamma} = \frac{1}{bs} - \frac{L_{CS}\varrho}{b} \tag{4}$$

and

$$\sigma\Theta = \frac{\alpha^2 G^2 b}{2s}\left[1 - \left(\frac{\sigma}{\sigma_S^*}\right)^2\right] \tag{5}$$

where $\sigma_S^* = \alpha G b / (L_{CS} s)^{1/2}$ and s is the particle spacing or grain size.

2.1.1 The Malygin Model

Malygin [8] took into account processes of multiplication of dislocations at both impenetrable obstacles and forest dislocations and process of dislocation annihilation due to cross-slip in a homogeneous material. The evolution equation in this case has the following form:

$$\frac{\partial \varrho}{\partial \gamma} = \frac{1}{bs} + \kappa_f \varrho^{1/2} - \kappa_a \varrho \tag{6}$$

where s is particle spacing or grain size, κ_f is the coefficient of the dislocation multiplication intensity due to interaction with forest dislocations and κ_a is the coefficient of the dislocation annihilation intensity due to cross slip. Finally he obtained the following equation which is suitable for an analysis of the experimental work hardening curve of polycrystals:

$$\Theta = \frac{\partial \sigma}{\partial \varepsilon} = \mathscr{A}/(\sigma - \sigma_y) + \mathscr{B} - \mathscr{C}(\sigma - \sigma_y) \tag{7}$$

where $\varepsilon = M^{-1}\gamma$ and the following substitutions were made:

$$\left.\begin{aligned} \mathscr{A} &= \tfrac{1}{2}M^3(\alpha G b)^2 \frac{1}{bs}; \\ \mathscr{B} &= \tfrac{1}{2}M^2 \alpha G b \kappa_f; \\ \mathscr{C} &= \tfrac{1}{2}M\kappa_a . \end{aligned}\right\} \tag{8}$$

Here M is Taylor factor ($M = 3.06$ for fcc metals) and $\alpha \approx 0.5$ is an interaction constant, which contains details of the deformation conditions ($\dot{\varepsilon}$ and T) and material properties (stacking fault energy γ_{sf}). The yield stress σ_y corresponds to the beginning of plastic deformation and comprises all contributions from the various hardening mechanisms.

2.1.2 The Lukáč and Balík Model

In many materials, Malygin's model [8] describes satisfactorily the whole work hardening curve at lower temperatures [9, 20] where only stage II and III hardening occurs. At intermediate temperatures (about $0.3T_m$, T_m being the melting temperature) there are deviations from the predictions of this model which indicate presence of some other recovery process in addition to cross-slip. Lukáč and Balík [9] assumed dislocation climb to be this additional process and derived the kinetic equation in the following form:

$$\frac{\partial \varrho}{\partial \gamma} = \frac{1}{bs} + \kappa_f \varrho^{1/2} - \frac{cL_{cs}}{b} - \frac{D_c b^2 \psi_c}{\chi k_B T \dot{\gamma}} \tau \varrho^{3/2} \tag{9}$$

where L_{cs} is the dislocation segment length recovered by one cross-slip event, c is the area concentration of the recovery sites in a slip plane, ψ_c is a fraction of the

dislocations which can be annihilated by climb of dislocations with jogs, χ is a parameter which gives the relation between dislocation climb distance w (i.e. distance between storage of a dislocation and its annihilation site) and the average dislocation spacing $1/\sqrt{\varrho}$ in the form $w = \chi/\sqrt{\varrho}$, τ is the shear stress, k_B is the Boltzmann constant and D_c is an abbreviation which includes the diffusion coefficient and the stacking fault energy. The stress dependence of the work hardening rate for polycrystals can be then written in the following form:

$$\Theta = \frac{\mathscr{A}}{\sigma - \sigma_y} + \mathscr{B} - \mathscr{C}(\sigma - \sigma_y) - \mathscr{D}(\sigma - \sigma_y)^3 \tag{10}$$

where the meaning of the parameters used is as follows:

$$\left.\begin{aligned} \mathscr{A} &= M^3(\alpha G)^2 \frac{b}{2s}\left(\frac{\dot{\varepsilon}}{\dot{\varepsilon}_1}\right)^{2/n}; \\ \mathscr{B} &= \frac{1}{2} M^2 \alpha G n \kappa_f \left(\frac{\dot{\varepsilon}}{\dot{\varepsilon}_1}\right)^{1/n}; \\ \mathscr{C} &= M \frac{cL_{cs}}{2b\varrho}; \\ \mathscr{D} &= M^{-2} \frac{\psi_c D_c b}{2\chi\alpha G k_B T \dot{\varepsilon}} \left(\frac{\dot{\varepsilon}}{\dot{\varepsilon}_1}\right)^{-1/n}. \end{aligned}\right\} \tag{11}$$

Here $\dot{\varepsilon}_1$ is a parameter and n is the stress exponent.

2.1.3 The Gottstein and Argon Model

The model [6] is designed for a cell-forming material. Gottstein and Argon took into account three basic recovery mechanisms: cross-slip, climb and mutual subboundary annihilation as a result of migration. Production of dislocations is accounted only for primary dislocations, *i.e.* in response to an external stress. In the absence of fundamental criteria for the density of other subsets of dislocation (like secondary dislocations, obstacle densities, dislocations in subboundaries etc.) a principle of similitude [31] is applied – the dislocation densities are assumed to be proportional to each other.

This access leads to the evolution equation of the average dislocation density in the following form [6]

$$\frac{\partial \varrho}{\partial \gamma} = \frac{\sqrt{\varrho}}{b\kappa} - \frac{L_R}{b}\varrho - \left(\frac{D_c}{\chi} + m\beta^2 b\tau_m\left[1 + \frac{\lambda}{\kappa}\right]\right)\frac{\varrho^2}{\dot{\gamma}} \tag{12}$$

where γ is the shear strain, $\dot{\gamma}$ is the shear strain rate, ϱ is the dislocation density, b is the Burgers vector, κ, λ, β and χ [6] are constants of the order of 1, m is the subboundary mobility, τ_m is the shear stress on the subboundary, L_R is the swept-up line length per recovery site [3] and D_c is the effective volume diffusion constant

for dislocation climb. The stress dependence of the work hardening coefficient can be then written in the form

$$\vartheta = \frac{\alpha G}{2\kappa} - \frac{L_R}{2b}(\tau - \tau_c) - \left(\frac{D_c}{\chi} + m\beta^2 b\tau_m\left[1 + \frac{\lambda}{\kappa}\right]\right)\frac{(\tau - \tau_c)^3}{2\alpha G b}\frac{1}{\dot{\gamma}} \tag{13}$$

where τ_c is the critical resolved shear stress. In the absence of climb and subboundary motion ϑ should decrease linearly with stress similarly as proposed by Kocks [3].

3.1.4 The Prinz and Argon Model

In this model [7] a simple one-dimensional cellular structure is considered with the width of cell interiors $2c$, width of cell walls h and periodicity $2a = 2c + h$. The shear strain is idealized to result from the glide motion of a single set of dislocations along parallel planes. Climb may be important only in the cell walls and then only associated with very short diffusion paths. Similitude [31] is invoked again, without furnishing any detail on how this similitude is established and maintained.

The total plastic resistance, τ, of a periodic assembly of cell interiors of dimensions $2c$ and cell walls of thickness $2(a - c)$ with individual total plastic resistances τ_1 and τ_2 is identical to the shear resistance of a set of periodic traction bearing cracks separated by ligaments of higher shear resistance. The problem has been solved by Bilby *et al.* [32], and for $(a - c) \ll a$ is simply

$$\tau = \tau_1 + \tau_2\left(\frac{a - c}{a}\right). \tag{14}$$

The strain hardening rate of the assembly then will be the weighted sum of the strain hardening rates of the individual regions

$$\vartheta = \frac{1}{G}\frac{\partial\tau}{\partial\gamma} = \frac{1}{G}\frac{\partial\tau_1}{\partial\gamma} + \frac{1}{G}\frac{\partial\tau_2}{\partial\gamma}\left(\frac{a - c}{a}\right) = \vartheta_1 + \vartheta_2\left(\frac{a - c}{a}\right). \tag{15}$$

In the intermediate temperature range the temperature dependent component of the glide plane resistance is absent and it is possible to write [7] for the cells

$$\vartheta_1 = \frac{1}{G}\frac{\partial\tau_1}{\partial\gamma} = C_1 - C_2\left(\frac{\tau_1}{G}\right) \tag{16}$$

$$C_1 = \frac{\pi r_0}{K^2}(\beta_1 + \beta_2 x^{1/2}) \tag{17}$$

$$C_2 = \frac{L_a}{2bK^2}. \tag{18}$$

and similarly the strain hardening rate of the cell walls is given as follows:

$$\vartheta_2 = \frac{1}{G}\frac{\partial \tau_2}{\partial \gamma} = C_3\left(\frac{\tau_1}{\tau_2}\right) - C_4\left(\frac{\tau_2}{G}\right)^{2i-1} \tag{19}$$

$$C_3 = \frac{1}{\sqrt{6}}\left(\frac{a}{a-c}\right)\left(\frac{\beta_1^2 x^{1/2}}{\beta_1 + \beta_2^2 x^{1/2}}\right) \tag{20}$$

$$C_4 = \frac{K_i}{\dot{\gamma}(b\beta_1)^{2(i-1)}}. \tag{21}$$

where β_1 and β_2 are constants in the order of 1, $x = \varrho_m/\varrho_1$ is the ratio of the mobile dislocation density ϱ_m to the total dislocation density, $r_0 \approx 0.5$ is the relative radius of this impenetrable regions as compared with the mean spacing, $l_1 = 1/\varrho_1$, of the forest dislocation network, K describes the portion of the obstacle network which is impenetrable to dislocations, L_a is line length cancellable per each loop during interaction of dislocation loops, i is 2 for lattice diffusion and 3 for core diffusion and K_i express, in respective cases, the time rates of dislocation density decays due to diffusion.

2.2 Conditions for Discontinuous Flow

A very detailed general overview of the problematics of unstable plastic deformation has been recently given by M. Zaiser and P. Hähner [33] together with a basic decription of various theoretical concepts which have appeared in the literature in the past decades. Therefore we will present at this place only some basic equations of the model of Kubin and Estrin [27] which has a direct connection to the present work.

2.2.1 The Model of Kubin and Estrin

The model developed by Kubin and Estrin [27] is based on the variation of the densities of mobile and forest dislocations with strain. Using the Orowan equation the plastic shear strain rate $\dot{\gamma}$ is given by

$$\dot{\gamma} = b\varrho_m\varrho_f^{-1/2}/t_w = \Omega/t_w \tag{22}$$

where ϱ_f and ϱ_m is the density of forest and mobile dislocations, respectively, b is the Burgers vector and t_w is the dislocation waiting time at forest obstacles. The elementary incremental strain Ω expressing the deformation produced when all mobile dislocations undergo a successful activation jump, is a strain dependent quantity. The strain dependence of the elementary strain can be obtained from the two coupled differential equations (for details see [27])

$$\partial\varrho_m/\partial\gamma = C_1/b^2 - C_2\varrho_m - (C_3/b)\,\varrho_f^{1/2}, \tag{23}$$

$$\partial\varrho_f/\partial\gamma = C_2\varrho_m + (C_3/b)\,\varrho_f^{1/2} - C_4\varrho_f. \tag{24}$$

Here C_1 is related to the multiplication of mobile dislocations, C_2 expresses the mutual annihilation of mobile dislocations, C_3 is related to the immobilization of mobile dislocations at forest dislocations and C_4 is connected to dynamic recovery.

The dislocation densities tend to saturation. It is assumed [27] that the shear stress τ can be expressed as a sum of two components:

$$\tau = \tau_0 + \tau_a = \tau_0 + f_0\{1 - \exp\left[-(t_w/t_0)^{2/3}\right]\} = \tau_0 + f_0\{1 - \exp\left[-(\Omega/t_0\dot{\gamma})^{2/3}\right]\}. \quad (25)$$

The first component τ_0 corresponds to an "ordinary" thermally activated process in the absence of dynamic strain ageing and the second one τ_a results from the dynamic strain ageing mechanism, f_0 is the maximum stress increase produced by the ageing mechanism and t_0 is the relaxation time which, in this case, depends on the binding energy between a solute atom and a dislocation, on the solute concentration and on the diffusion coefficient of the solute atoms. In this case the strain rate sensitivity of the shear stress $S = (\partial\tau/\partial \ln \dot{\gamma})_\gamma$ is given by the equation

$$S = S_0 - \frac{2}{3} f_0(\Omega/t_0\dot{\gamma})^{2/3} \exp\left[-(\Omega/t_0\dot{\gamma})^{2/3}\right] \quad (26)$$

where $S_0 = (\partial\tau_0/\partial \ln \dot{\gamma})_\gamma$. The condition for the occurrence of the PLC-effect is expressed by the condition that $S \leq 0$ in equation (26). The appearance of PLC-effect is then given by the condition

$$X_1^{3/2} t_0\dot{\gamma} \leq \Omega(\gamma) \leq X_2^{3/2} t_0\dot{\gamma}, \; X = \left(\frac{t_w}{t_0}\right)^{2/3}. \quad (27)$$

2.2.1.1 Balík and Lukáč's adoption of the model. Balík and Lukáč [30] adopted the model of Kubin and Estrin [27] to their experimental data. The condition (27) for the range of strain rates within which serrations can occur can be expressed in the form

$$\Omega(\gamma)/t_0 X_2^{3/2} \leq \dot{\gamma} \leq \Omega(\gamma)/t_0 X_1^{3/2}. \quad (28)$$

The limit cases of inequality (28) define the critical conditions for the onset or disappearance of the PLC effect. The critical states given by the two solutions X_1 and X_2 of equation (27) may also be called nonsaturated and saturated ones. If the $\Omega(\gamma)$ profile has a maximum with respect to strain, both X_1- and X_2- critical conditions can be met at two strains, one of these strains behaving thermally and the second "anti-thermally". The main part of the temperature effect enters through the relaxation time t_0, which is inversely proportional to the diffusion coefficient. Neglecting, at this time, the possible strain rate and temperature dependences of X_1, X_2 and Ω, the strain rate and temperature affect all critical conditions through the quantity $t_0(T) \cdot \dot{\gamma}$ [30]. This means that all features of the model of Kubin and Estrin [27] for a given strain rate and various temperatures should appear at a given temperature and various strain rates as well.

If we restrict ourselves to the low strain limit, whose condition is governed by the equation

$$\dot{\gamma}_c = \Omega(\gamma)/t_0 X_2^{3/2} = \Omega(\gamma)/C_5 \quad (29)$$

and, according to considerations made by Balík and Lukáč [30], assume that C_5 is strain independent parameter for a given temperature, then the $\dot{\gamma}_c(\gamma)$ and $\Omega(\gamma)$ curves should have the same shape. In order to verify this prediction quantitatively we convert the set of differential equations (23) and (24) into one equation of second order for the elementary strain Ω. Using equation (29) we obtain the following differential equation for the critical strain rate

$$\frac{\partial^2\dot{\gamma}_c}{\partial\gamma^2} = \left(\frac{C_4}{2} - C_2\right)\frac{\partial\dot{\gamma}_c}{\partial\gamma} + \left(C_2 + \frac{\kappa_3}{\dot{\gamma}_c}\right)\delta + \left(\frac{\delta}{\dot{\gamma}_c}\right)\cdot\frac{\kappa_1\delta + \left(\frac{3}{2}C_2\dot{\gamma}_c^2 + \kappa_3\dot{\gamma}_c - \kappa_1\right)\frac{\partial\dot{\gamma}_c}{\partial\gamma}}{\frac{C_2}{2}\dot{\gamma}_c^2 + \frac{\kappa_3}{2}\dot{\gamma}_c - \kappa_1} \tag{30}$$

where the following notation is introduced

$$\delta = \frac{\partial\dot{\gamma}_c}{\partial\gamma} + \kappa_3 - \left(\frac{C_4}{2} - C_2\right)\dot{\gamma}_c\,, \tag{31}$$

$$\kappa_1 = C_1/C_5^2,\ \kappa_3 = C_3/C_5 \tag{32}$$

Equation (30) may be simply compared with the experimental data of the low strain limit assuming the parameters in equation (30) are strain rate independent.

3. Experimental Procedure

3.1 Manufacturing of Samples

For the experiments three different aluminium based alloys were used. Mechanical and thermal processing and dimensions of the samples are described in the following list:

- Commercial aluminium alloy of type 7020 with 5 wt.% Zn and 1.2 wt.% Mg. In the following text will be referred to as Al–5%Zn–1.2%Mg. Samples of 21.5 mm gauge length and 8 mm width were cut out of 1.5 mm thick hot rolled sheets, solution treated at 485°C for one hour in air and quenched into water. One set of samples was stored in liquid nitrogen before testing (AZM-I) and the second one was aged at room temperature for 25 days prior to testing (AZM-II).
- Pure aluminium alloy with 4.8 wt.% Mg supplied by Alusuisse Lonza. In the following text will be referred to as Al–4.8%Mg. Three sets of samples were manufactured from three different (independently rolled) sheets. The gauge length was 49 mm by all samples from the first set (AM-I), whereas several types of samples with the gauge lengths varying from 28 to 51 mm were machined in the case of second set (AM-II). By the third set of samples (AM-III) the gauge length was constant again — 35 mm by all samples. The active part of the samples was 6 mm wide in all cases. Samples were solution treated for 1.5 hour at 500°C: the first set of samples (AM-I) in air, the second (AM-II) in high vacuum

($p < 5 \times 10^{-6}$ mbar) and the third (AM-III) in an argon atmosphere, and quenched consequently into distilled water. All three sets of samples were stored in liquid nitrogen before testing. The time of storage was up to 200 days.

- Pure aluminium alloy with 2.57 wt.% Mg. In the following text will be referred to as Al–2.6%Mg. Alloy was prepared from a commercial aluminium high purity base 1070. Samples of 49 mm gauge length and 6 mm width were cut out of 1.0 mm thick hot rolled sheets. The thermal treatment was same as by the first set of Al–4.8%Mg alloy (AM-I). The samples were stored in liquid nitrogen before testing.

Chemical composition of the samples is given in table 1. The annealing temperature T_A, annealing time t_A, working medium of the furnace, mean grain size d_g and conditions of storage are given in table 2. The mean grain size d_g was determined from the optical micrographs by the linear intercept method.

Alloy	Fe	Si	Mg	Zn	Ti	Na	Cr	Mn	Cu
	[wt. %]								
Al–4.8%Mg	0.03	0.02	4.8	0.005	0.01	–	–	–	–
Al–2.6%Mg	0.15	0.05	2.57	0.05	0.01	5×10^{-4}	–	–	–
Al–5%Zn–1.2%Mg	0.3	0.15	1.2	5.0	0.1	–	0.2	0.25	0.2

Table 1
Composition of the alloys.

Alloy	T_A [K]	t_A [min]	Medium	d_g [μm]	Storage
Al–4.8%Mg I	773	90	air	85 ± 9	liquid N_2
Al–4.8%Mg II	773	90	vacuum	91 ± 9	liquid N_2
Al–4.8%Mg III	773	90	argon	87 ± 8	liquid N_2
Al–2.6%Mg	773	90	air	66 ± 4	liquid N_2
Al–5%Zn–1.2%Mg I	758	60	air	22 ± 7	liquid N_2
Al–5%Zn–1.2%Mg II	758	60	air	22 ± 7	25 days at RT

Table 2
Conditions of thermal treatment, resulting grain size and conditions of storage of the samples.

3.2 Observation of Microstructure

Microstructure of both underformed and deformed samples of Al–4.8%Mg and Al–2.6%Mg alloys was investigated by transmission electron microscopy (TEM). For manufacturing of foils a TENUPOL 2 device and electrolyte with composition 10% perchloric acid, 20% glycerol and 80% ethanol was used. The working current was about 200 mA at 255 K. TEM observations were realized in a JEOL 2000 FX microscope.

3.3 Tensile Tests

The tensile tests were carried out in an INSTRON 1185 machine. For the temperatures below room temperature an ethanol bath was used. The bath was cooled by blowing of liquid nitrogen through a cooper helix plunged into the bath. Temperature was measured simultaneously by an ethanol thermometer and by a NiCr–Ni thermocouple. Accuracy of this measurement was better than ± 1 K. Stability of temperature was better than ± 2 K at the lowest temperature used for experiments and typically about ± 1 K.

For the higher temperatures an electric furnace was used. Temperature was measured by a NiCr–Ni thermocouple with accuracy better than ± 3 K. Stability of temperature was in this case better than ± 1.5 K. In order to stabilize the whole experimental set-up properly at higher temperatures without an undefined annealing of the sample during this stabilization, the furnace was heated for several hours at the test temperature, then the sample was mounted and the furnace was stabilized for 30 minutes (after reaching the test temperature) with the sample and the experiment was started afterwards.

For the data acquisition a HP-85B personal computer and later an IBM AT compatible computer was used. The rate of data sampling was set to 0.3% of the full scale load in the case of experiments controlled by the HP-85B personal computer, whereas it varied from 2 ms to 20 s in the case of IBM AT compatible PC. This means that two diffrenet modes of data sampling were used — constant force increment and constant time interval — in respective cases.

3.4 X-Ray Diffraction

3.4.1 Experimental set-up

X-ray diffraction experiments were performed with both undeformed and deformed samples of Al–4.8%Mg and Al–2.6%Mg alloys with the aim to determine the average dislocation density ϱ from the deformation-induced peak broadening. A special double-crystal diffractometer with wavelength compensation was used. For detailed description see [35, 36]. The primary X-ray beam was monochromatised by a symmetrically cut plane Ge monochromator using the (444) reflection. The monochromator was tuned to the $CuK\alpha_1$ line. Wavelength dispersion of the beam was about $\Delta\lambda/\lambda = 3 \times 10^{-4}$. The appropriately collimated and monochromatic X-ray beam impinged on the flat sample under a divergence angle of about 10 seconds of arc. By a slit mechanism selected single grains were illuminated in a polycrystalline sample. The scattered radiation was registered by a linear position-sensitive X-ray detector of OED-50 type (Braun, München, Germany). The instrumental X-ray peak broadening was negligible if compared with the measured peak width.

3.4.2 Evaluation Procedure

Ungár, Groma and Wilkens [37, 38] have shown that within the formalisms of the kinematical scattering of X-rays and the linear elasticity theory of dislocations

the Fourier coefficients, $A(n)$, of a X-ray peak-profile can be written in the following form:

$$\ln A(n) = -\varrho C n^2 \ln \frac{R_e}{n} + \frac{\Delta\varrho^2}{2} n^4 \ln \frac{R_2}{n} \ln \frac{R_3}{n} - iP_0 n^3 \ln \frac{R_1}{n} \tag{33}$$

where ϱ is the average dislocation density, C is a geometric factor correlating the type of dislocation with the diffraction vector, n is a Fourier parameter which is of the length dimension, $\Delta\varrho^2$ is the mean quadratic fluctuation of the dislocation density, P_0 is proportional to the dipole-polarization moment of the dislocation structure and R_e is the effective outer cut-off radius of dislocations. R_1, R_2 and R_3 are parameters of length dimension which are of no relevance in the present case when only the average dislocation density is to be determined. Equation (33) is based on a microscopis model where the dislocations are the only defect which causes the peak broadening.

For the purpose of evaluation of the measured X-ray profiles, we can transcribe equation (33) into a simplified form as follows:

$$\ln |A(n)| \approx -\varrho^* n^2 \ln \frac{R_e}{n}. \tag{34}$$

The true dislocation density ϱ is related to the formal dislocation density ϱ^* according to the following equation [37, 38, 39]:

$$\varrho = \frac{2}{\pi} \frac{\varrho^*}{g^2 b^2 C} = k\varrho^*, \tag{35}$$

where g and b are the magnitudes of the diffraction and Burgers vectors, respectively, and $k = 2/\pi g^2 b^2 C$ is transformation coefficient. If there are more than one slip system active (and this is always the case in a polycrystalline material) it is necessary to use a weighted average $\bar{C}$ instead of C [39]. For the values of C the isotropic values were taken into account as given by Wilkens [40] and Borbély [41] for the g_{200} and g_{220} diffraction vectors, respectively. The resulting values of the transformation coefficient were then $k = 1.34$ and $k = 1.06$ for g_{200} and g_{220}, respectively.

4. Experimental Results

4.1 Tensile Tests

The digitalized data stored by computer in the form $F(t)$, where F is force and t is time, were further evaluated using the SigmaPlot SP5 scientific graphing program. From the force-total elongation curves $F(\Delta l_{tot})$, where

$$\Delta l_{tot} = v_d t \tag{36}$$

and v_d is the crosshead speed, the (true)stress-(plastic)strain curves $\sigma(\varepsilon)$ were computed according to following definitions

$$\sigma = \frac{F}{S}, \tag{37}$$

$$\varepsilon = \ln\left(1 + \frac{\Delta l_{\text{tot}} - \Delta l_{\text{elast}}}{l_{\text{i}}}\right), \tag{38}$$

where S is the true cross-section of the sample, Δl_{tot} is total elongation of the sample, Δl_{elast} is elastic part of elongation and l_{i} is initial length of the sample. The true plastic strain ε can be transformed into the shear strain γ according to equation $\gamma = M\varepsilon$ where $M = 3.06$ is the Taylor factor for f.c.c. metals. The true plastic strain has been chosen with respect of the conclusions made by Balík *et. al.* [42] (we suppose it to be the most appropriate description in the case of penetrating slip systems in grains which are active in the present case).

4.1.1 Serrated Flow

The PLC effect was observed for all three alloys at the strain rates at room temperature with the exception of the aged samples of Al–5%Zn–1.2%Mg alloys, where the formation of Guinier-Preston zones inhibits the serrations. The (true)stress-(plastic)strain, $\sigma(\varepsilon)$, curves which were computed from the digitalized experimental force-time curves are shown in figure 1 for the Al–5%Zn–1.2%Mg alloy at two different strain rates and in figure 2 for the Al–4.8%Mg alloy at five different strain rates. All the curves were measured at room temperature.

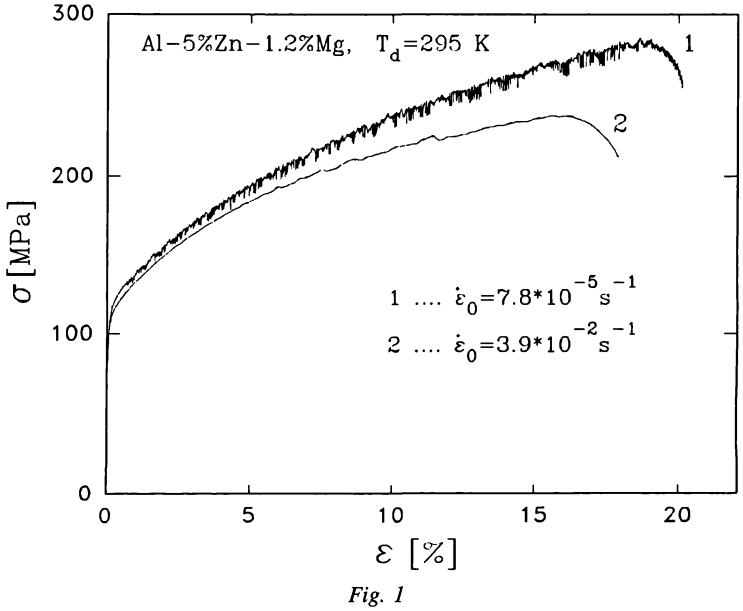

Fig. 1

Experimental stress-strain curves of the Al–5%Zn–1.2%Mg alloy for different initial strain rates $\dot{\varepsilon}_0$ at room temperature.

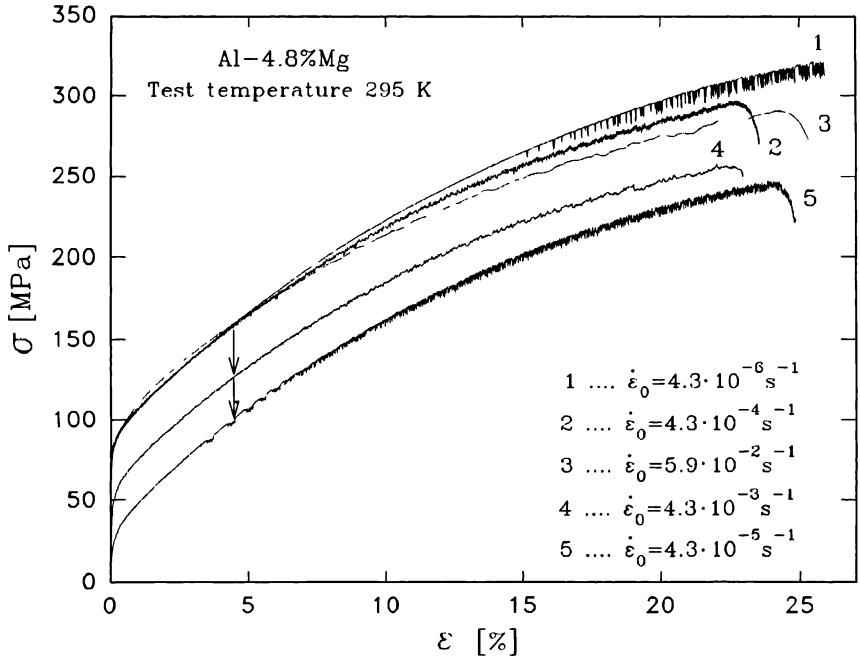

Fig. 2

Experimental stress-strain curves of the Al–4.8%Mg alloy for five different initial strain rates $\dot{\varepsilon}_0$ at room temperature. The curves denoted as "4" and "5" are vertically shifted at 30 and 60 MPa, respectively, to the lower values relatively to the curves "1" to "3".

In figure 2 the following facts should be mentioned: i) the stress-strain curves exhibit very high work hardening which is in accordance with experimental results of Chmelík *et al.* [43, 44] on Al–3%Mg and Al–2.92%Mg–0.38%Mn alloys; ii) no transition from the jerky to the smooth regime is observed; iii) negative SRS is observed at higher strains ($\varepsilon > 5\%$) in the whole range of strain rates. This fact is further confirmed by the strain rate dependence of the saturated stress σ_s as presented in figure 3. The saturated stress is obtained as an intersection of the extrapolated work hardening rate – flow stress, $\Theta(\sigma)$, curve for large stresses with the $\Theta = 0$ axis. The work hardening coefficient Θ is defined by equation (1). For the curves where the PLC effect of the type C (the definitiobn see below) occured, the saturated stress was determined from the envelope curve, whereas in the case of the A and B types it was determined from the "average" curve (parabolic regression). For details on this procedure see the next section. It can be seen that, with exception of the highest strain rate, the saturated stress decreases with increasing strain rate which means that a negative strain rate sensitivity of the flow stress can be expected in this range.

The observed strain rate dependence of the saturated stress in the Al–4.8%Mg alloy is in accordance with the results of Mukai *et al.* [45], who tested five

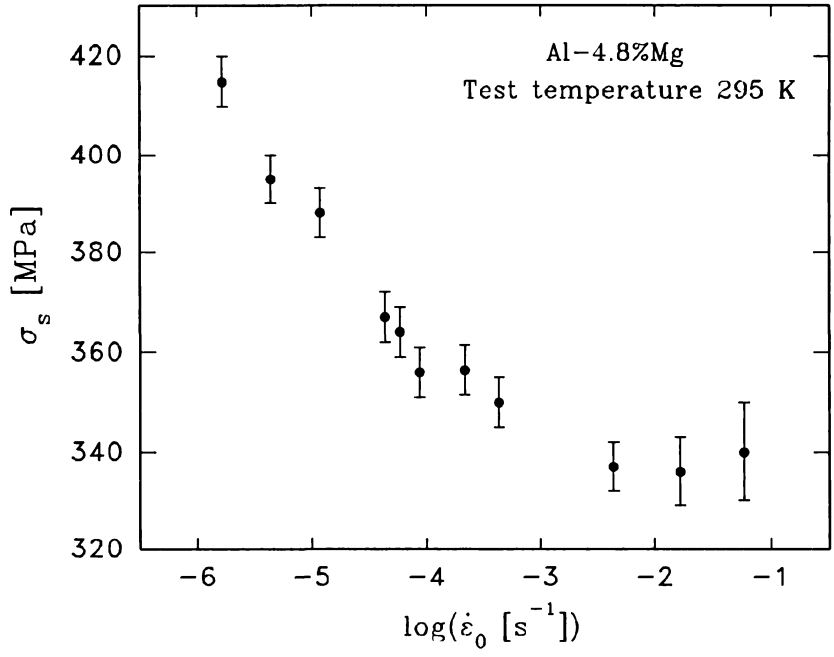

Fig. 3
Strain rate dependence of the saturated stress for Al–4.8%Mg alloy at room temperature.

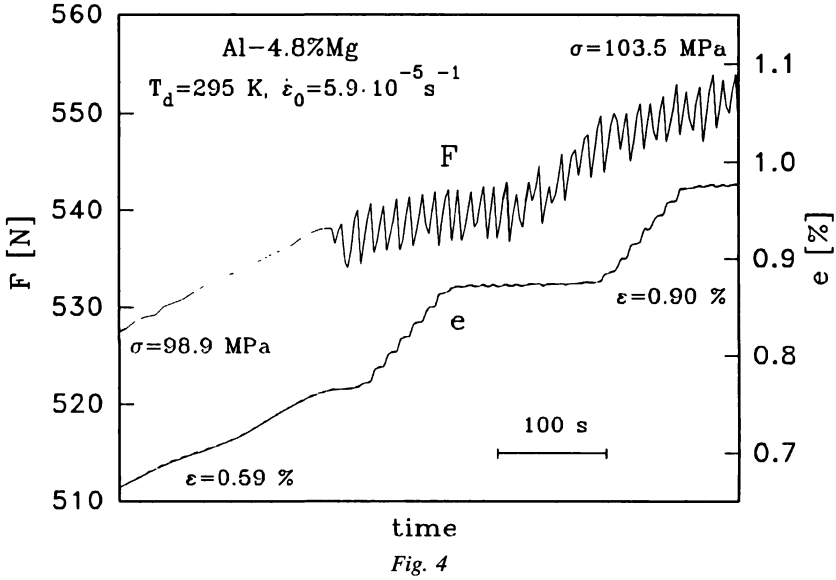

Fig. 4
Evaluation of the onset critical strain from coincidence of load (F) and elongation (e) data. The values of stress and strain are indicated for the border points of load and elongation signals.

aluminium-magnesium alloys with Mg concentration ranging from 1.8% to 8.4% and have reported a decreasing strain rate dependence of the maximum flow stress for the initial strain rates ranging from $10^{-4}\,s^{-1}$ to $10^{2}\,s^{-1}$. Under the assumption that no prenature crack of the sample occurs, the course of the strain rate dependences of the maximum stress and saturated stress should be qualitatively the same.

The critical strain for the onset of PLC effect has been determined from the coincidence of irregularities in the load cell and extensometer signals. Occasional irregularities in the load signal are ignored if the extensometer shows no elongation bursts or waves. An example of the coincidence of signals at the moment of reaching critical strain is shows in figure 4 for the Al–4.8%Mg alloy deformed and $\dot{\varepsilon}_0 = 5.9 \times 10^{-5}\,s^{-1}$ at room temperature. Figures 5 and 6 show the strain rate dependence of the critical strains for the plastic instability limit $\varepsilon_c(\log \dot{\varepsilon}_c)$ for the Al–4.8%Mg and Al–2.6%Mg alloys, respectively. The results are very similar to those obtained by Balík and Lukáč for the Al–3%Mg alloy [30] with the exception that no PLC effect was observed in the present case for the strains below $\approx 0.2\%$ and no transition from jerky to smooth flow has been observed. The classification of the PLC types (A, B and C) is made consistently with literature [28, 46, 47].

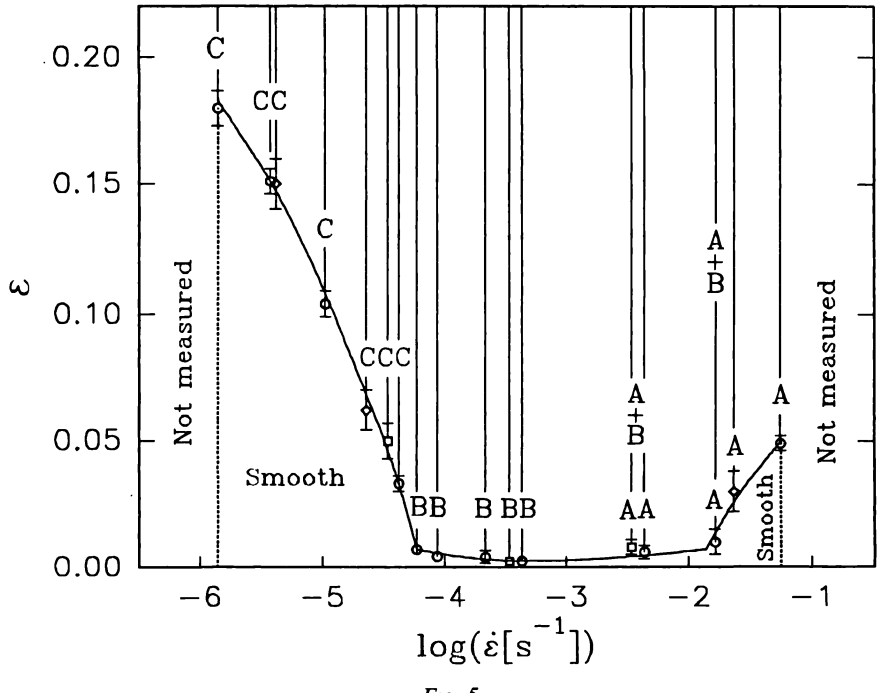

Fig. 5

Strain rate dependence of the critical strains for the Al–4.8%Mg alloy at room temperature. The symbols ○, □ and ◇ correspond to sample sets AM-I, AM-II and AM-III, respectively.

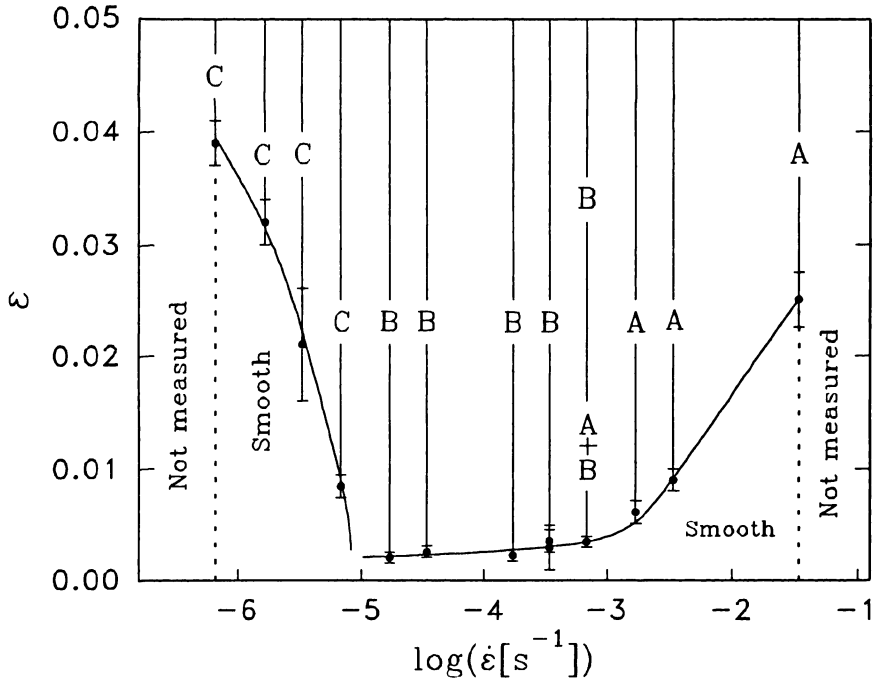

Fig. 6
Strain rate dependence of critical strains for the Al–2.6%Mg alloy at room temperature.

The behaviour D, E and F as described in [47] was not observed. Both A and B serrations can be characterized by a rise above the undisturbed stress-strain curve whereas C serrations only fall below the undisturbed curve. In figure 2 the curve denoted as "3" exhibits the A serrations, curve "2" the B serrations, curve "4" the A+B serrations and finally curves "1" and "5" the C serrations. Nevertheless, the various types of serrations have no direct connection to the present work and will not be, therefore, discussed in more details.

In the case of the Al–5%Zn–1.2%Mg alloy the observed values of the critical strains ε_c are in good correspondance with Pink [46, 48] who used the same material. Small differences can be explained by the strong effect of annealing of the samples at room temperature [46] because this annealing pratically occurs during the mounting of the sample into the grips, too, and the time of mounting is not invariant. In acordance with this fact, significantly better correspondence with the results of Pink [46] was obtained by the samples which were deformed immediately or within several hours after the thermal treatment. This makes the Al–5%Zn–1.2%Mg alloy unsuitable for quantitative checks [49].

Kumar [50] has recently investigated the temperature dependence of the onset strain in Al–5%Mg alloy. We can compare his experimental results [50] with our

data for the Al–4.8%Mg alloy. Figure 7 shows the temperature dependence of ε_c in the entire range of serrated flow as was reported by Kumar [50] for Al–5%Mg alloy deformed at the initial strain rate $\dot{\varepsilon}_0 = 10^{-4}\,s^{-1}$. In the same graph our results for Al–4.8%Mg alloy deformed at the initial strain rate $\dot{\varepsilon}_0 = 3.4 \cdot 10^{-4}\,s^{-1}$ are plotted. It can be seen that the character of the temperature dependences is very similar. The values of the critical strain ε_c observed in the present case for the Al–4.8%Mg alloy fall systematically below the values observed by Kumar in the case of the Al–5%Mg alloy. The difference is higher at higher temperatures (that means in the 'inverse' branch of the plot) whereas at room temperature the difference is relatively small — $\varepsilon_c \approx 0.7\%$ for the initial strain rate $\dot{\varepsilon}_0 = 6.7 \times 10^{-4}\,s^{-1}$ in the case of Kumar compared with $\varepsilon_c \approx 0.25\%$ for the initial strain rate $\dot{\varepsilon}_0 = 3.4 \times 10^{-4}\,s^{-1}$ in the present case. We assume that this difference can be attributed to the different composition, processing and thermal treatment (In the present case the samples were solution treated at 500°C for 1.5 h whereas in the case of Kumar [50] the solution treatment was done at 350°C for 1 h.) of the samples in respective cases.

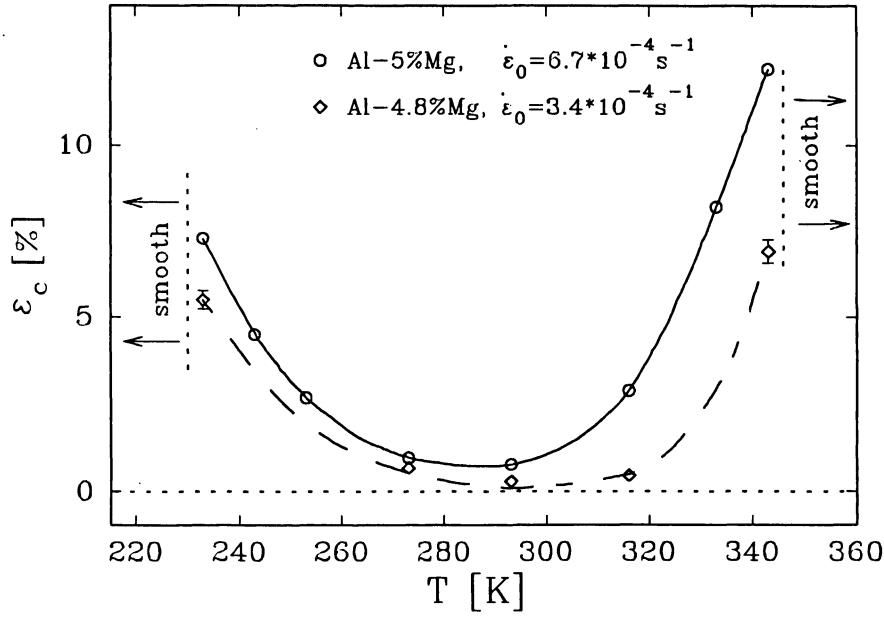

Fig. 7
Temperature dependence of the critical strain ε_c for Al–4.8%Mg and Al–5%Mg [50].

We assume that the observed "inverse" behaviour of the onset of jerky flow (i.e. the increase of the critical strain with temperature) above room temperature can be attributed to the dislocation mechanism as described in the model of Kubin and

Estrin [27, 28] and that, in the present case, the possible effect of precipitates can be neglected. This assumption is based on two facts: i) no effect of precipitation on the critical strain was observed by Kumar [50] for the Al–5%Mg alloy; ii) TEM observation of both undeformed and deformed samples showed merely a very small amount of Al_2Mg_3 precipitates in the case of Al–4.8%Mg alloy whereas no precipitates were observed in Al–2.6%Mg alloy. Nevertheless, the 'inverse' behaviour of critical strain was very similar for both Al–Mg alloys investigated in the present case, as well as the Al–5%Mg alloy investigated by Kumar [50].

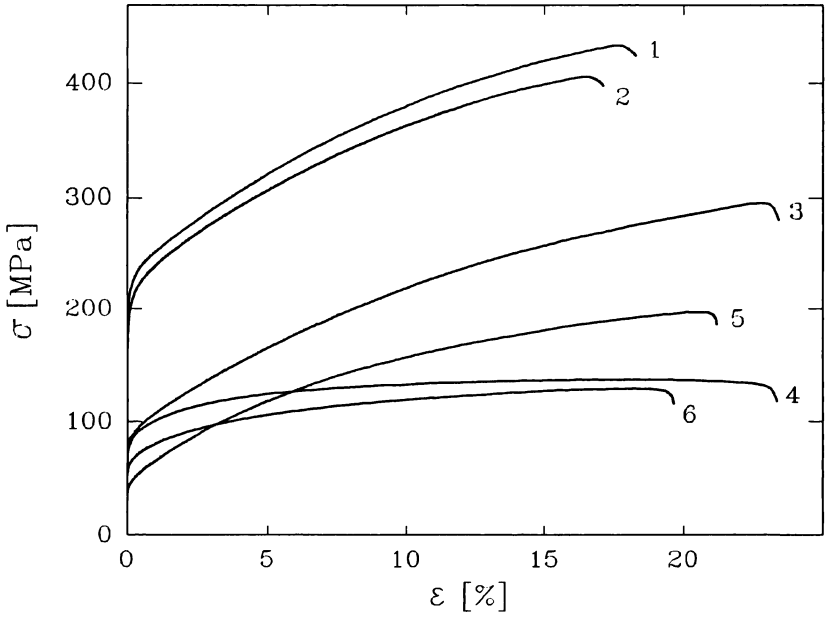

Fig. 8

Experimental (smoothed) stress-strain curves: (1.) Al–5%Zn–1.2%Mg alloy, test temperature T_d = 193 K, initial strain rate $\dot{\varepsilon}_0 = 7.8 \times 10^{-4}\,s^{-1}$; (2.) Al–5%Zn–1.2%Mg, T_d = 295 K, $\dot{\varepsilon}_0 = 7.8 \times 10^{-4}\,s^{-1}$; (3.) Al–4.8%Mg, T_d = 295 K, $\dot{\varepsilon}_0 = 4.3 \times 10^{-4}\,s^{-1}$; (4.) Al–4.8%Mg, T_d = 523 K, $\dot{\varepsilon}_0 = 4.3 \times 10^{-4}\,s^{-1}$; (5.) Al–2.6%Mg, T_d = 295 K, $\dot{\varepsilon}_0 = 3.4 \times 10^{-4}\,s^{-1}$; (6.) Al–2.6%Mg, T_d = 473 K, $\dot{\varepsilon}_0 = 3.4 \times 10^{-4}\,s^{-1}$.

4.1.2 Work Hardening

Both smooth and serrated stress-strain curves were used for the evaluation of work hardening parameter Θ: By the serrated curves an envelope curve or 'average' curve (quadratic regression) were used in order to smoothe the experimental data in the case of "C" or "B" serrations, respectively. The examples of the results of this two respective procedures are shown in figures 9 and 10 for B and C serrations, respectively. The smoothed stress-strain curves for the three alloys at five different strain rates and deformation temperatures are shown in figure 8.

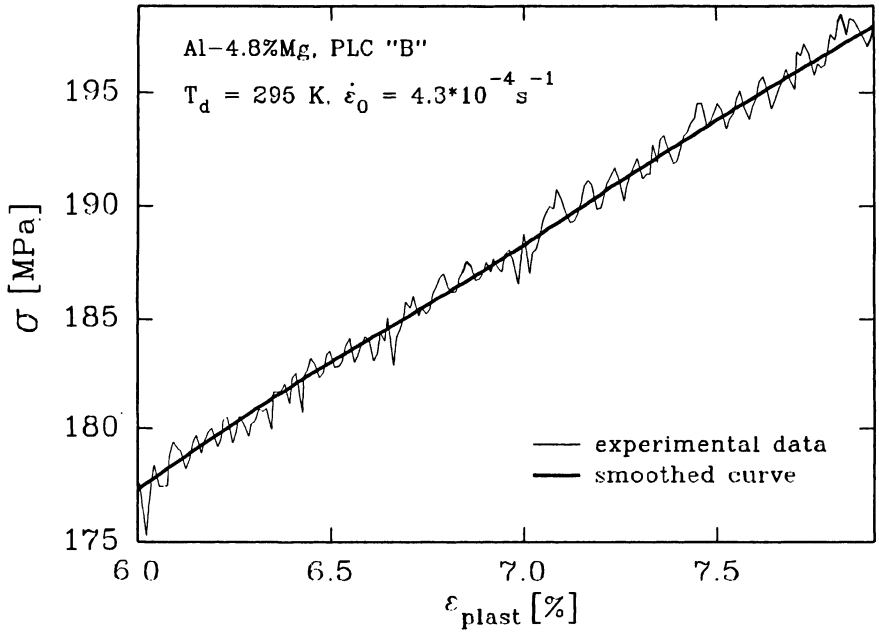

Fig. 9 Result of the smoothing procedure in the case of B serrations.

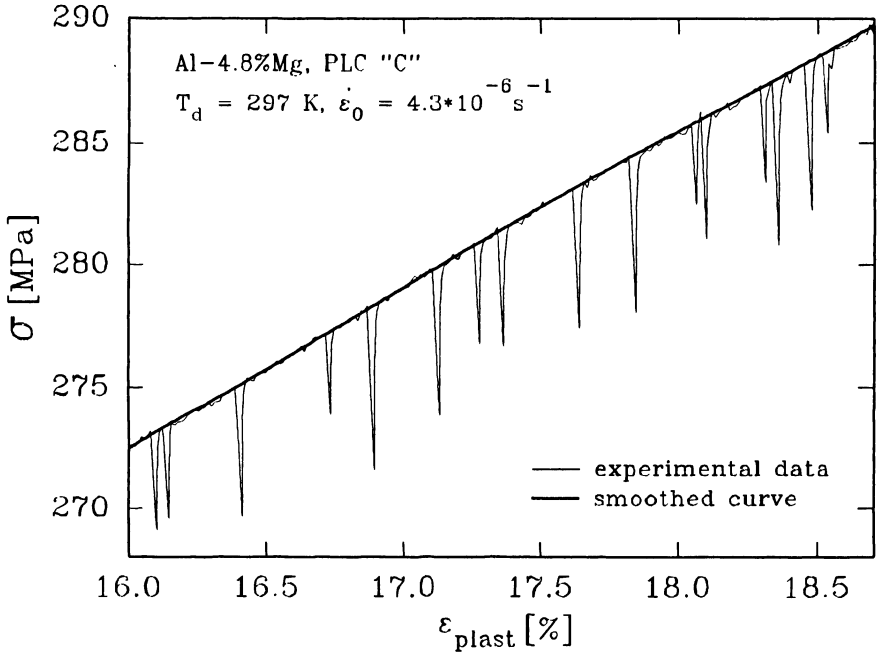

Fig. 10 Result of the smoothing procedure in the case of C serrations.

The stress dependences of the work hardening coefficient $\Theta(\sigma)$ were computed by numerical derivation of the experimental stress-strain curves. The number of points in parabolic regression was increased until the $\Theta(\sigma)$ curve became smooth. The influence of the number of points used for derivation was checked — no systematic effect was observed. The theoretical models described in the second section were then fitted to, in such way obtained, $\Theta(\sigma)$ curves. In the case of the Malygin's, Lukáč and Balík's and Gottstein and Argon's model the Marquardt least square method involved in the SigmaPlot 5.0 program was used. For the Prinz and Argon's model a special program in PASCAL was developed. The main part of the program is the simplex minimization procedure (Nelder-Mead method) which is described in detail in the Nash's book [51]. The PASCAL source file of the simplex procedure, which represents the main part of the program, was taken from the Celý's text-book [52]. The function which is minimized is the sum of relative square mistakes of the theoretical hardening curve described by the equations (15)—(19) as compared with the experimental work hardening curve. This function ("norm") is computed in following way: For a given set of parameters $C_1 - C_4$, σ_y (yield stress), $(a - c)/a$ (geometrical characterization of the celular structure) and $(\tau_1/\tau_2)_0$ (ratio of the stresses in the cells and in the walls on

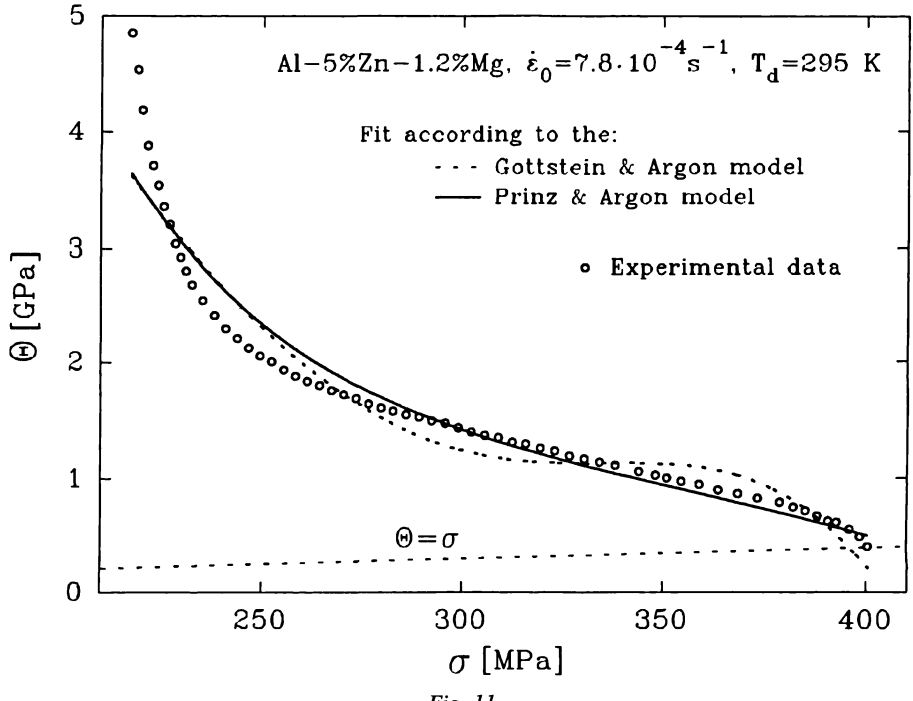

Fig. 11

Result of fitting the Gottstein and Argon model [6] and Prinz and Argon model [7] for the Al–5%Zn–1.2%Mg alloy deformed at T_d = 295 K at the initial strain rate $\dot{\varepsilon}_0 = 7.8 \times 10^{-4}\ s^{-1}$.

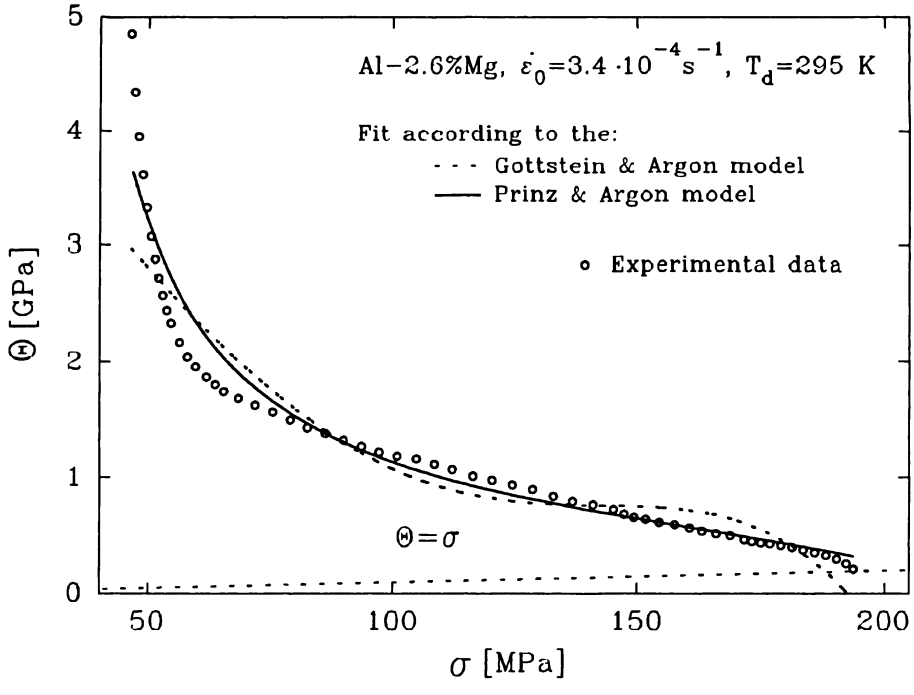

Fig. 12

Result of fitting the Gottstein and Argon model [6] and Prinz and Argon model [7] for the Al–2.6%Mg alloy deformed at T_d = 295 K at the initial strain rate $\dot{\varepsilon}_0 = 3.4 \times 10^{-4}\,s^{-1}$.

the beginning of plastic deformation) the equations (16) and (19) were numerically integrated (in iterations) until the total stress exceeded the maximum stress of the experimental curve and the step of integration was decreased in loop until the desired difference between following final stresses (in the two following runs of the loop) was satisfied. In such way obtained stress-strain curve was then derived numerically and compared with the numerical derivation of the experimental stress-strain curve and the "norm" was determined. Minimization was stopped under the condition, that the values of all parameters in the following iterations of simplex procedure were equal at all places.

Results of the fits of the Gottstein and Argon model [6] and Prinz and Argon model [7] for the Al–5%Zn–1.2%Mg alloy deformed at T_d = 295 K at the initial strain rate $\dot{\varepsilon}_0 = 7.8 \times 10^{-4}\,s^{-1}$ and for the Al–2.6%Mg alloy deformed at T_d = 295 K at the initial strain rate $\dot{\varepsilon}_0 = 3.4 \times 10^{-4}\,s^{-1}$ are presented in the figure 11 and figure 12, respectively. From these figures it is obvious that both the model of Gottstein and Argon [6] and Prinz and Argon [7] describe the shape of the work hardening curves much worse than the models of Malygin [8] and of Lukáč and Balík [9] (see figures 13 to 16). Nevertheless, the model parameters obtained from the fit for the Al–5%Zn–1.2%Mg alloy in the case of the Prinz and Argon model:

$C_1 = (1.9 \pm 0.5) \times 10^{-2}$, $C_2 = 35 \pm 15$, $C_3 = 0.15 \pm 0.08$ and $C_4 = (3 \pm 2) \times 10^7$ are, with exception of the C_3 parameter, in a satisfactory agreement with the values predicted by Prinz and Argon [7] for aluminium at room temperature: $C_1 = 0.0214$, $C_2 = 20$, $C_3 = 0.0375$ and $C_4 = 2.53 \times 10^7$. The results of the fits at other test temperatures and/or different strain rates are very similar (for the Al–5%Zn–1.2%Mg alloy as well as the both Al–Mg alloys) which let us conclude that the models [6, 7] are not relevant in the present case. In the following we will confine to the models of Malygin [8] and Lukáč and Balík [9] only.

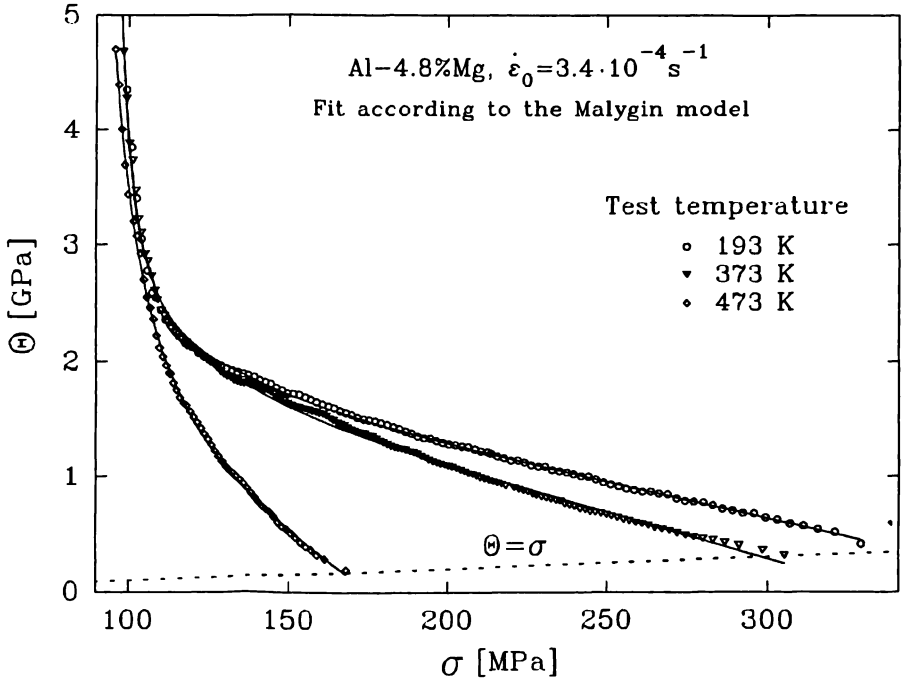

Fig. 13
Result of fitting the Malygin model for Al–4.8%Mg alloy deformed at the initial strain rate $\dot{\varepsilon}_0 = 3.4 \times 10^{-4}\ s^{-1}$ at various temperatures.

Results of fitting of the Malygin model for both Al–Mg alloys at various deformation temperatures are shown in figure 13 and figure 14, respectively. Results of fitting of the Lukáč and Balík model for the Al–5%Zn–1.2%Mg alloy at two different deformation temperatures are presented in figure 15. In figure 16 results of fitting of the Lukáč and Balík model are given for Al–4.8%Mg alloy and two different strain rates at room temperature. The detailed tables with the values of model parameters for both models have been presented in our previous papers [53, 54].

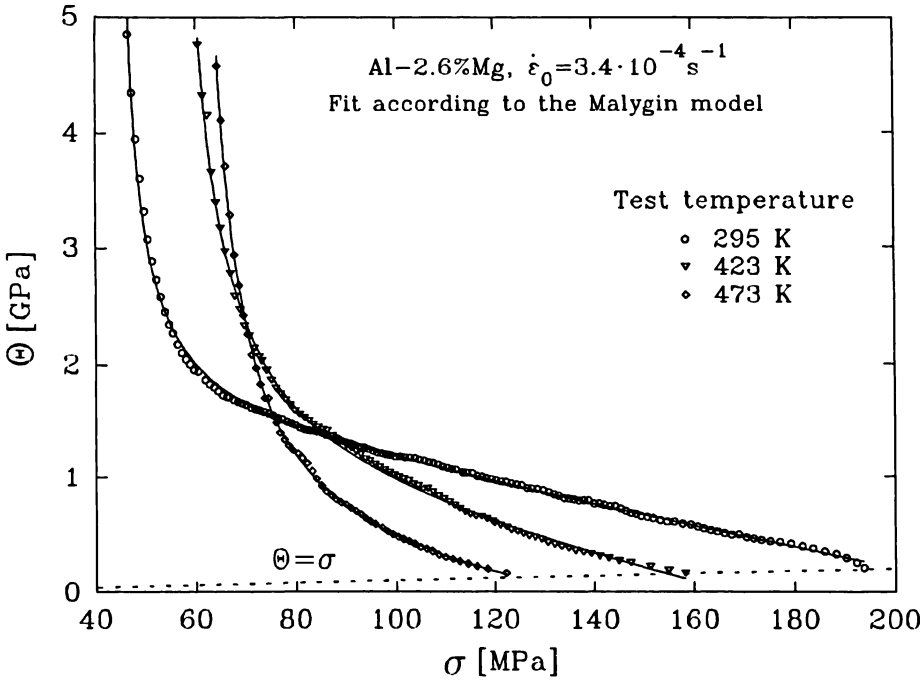

Fig. 14
Result of fitting the Malygin model for Al–2.6%Mg alloy deformed at the initial strain rate $\dot{\varepsilon}_0 = 3.4 \times 10^{-4}\ s^{-1}$ at various temperatures.

4.1.3 Stress Relaxations

The activation volume V was determined from stress relaxations performed during the tensile tests where for the rate of the stress decrease, $\dot{\sigma}$, at the beginning of stress relaxation holds [55]

$$-\dot{\sigma} = C \exp\{\varsigma\sigma\}, \tag{39}$$

where $\varsigma = V/kT$, k is Boltzmann constant and C is a constant. The plot of $\ln(\dot{\sigma})$ against σ for Al–2.6%Mg alloy tested at 423 K is shown in figure 17 for three various stresses at the beginning of stress relaxation.

In figure 18 a bilogaritmic plot of the stress dependence of the activation volume V_{act} for the three alloys is shown. We can mention that the activation volume decreases inversely with the stress in both Al–Mg alloys in the whole range of stresses, whereas in the Al–5%Zn–1.2%Mg alloy an obvious tendency towards reaching a stable value at higher stresses is observed.

4.1.4 X-ray Peak Profile Analysis

In figure 19 semilogaritmic plots of typical X-ray peak profiles obtained for Al–4.8%Mg alloy (second set) are shown. The two broader plots correspond to an

underformed (as annealed) sample and sample after deformation to fracture at 523 K, respectively. For a comparison, a profile corresponding to a perfect silicon crystal (400 reflection) is also given in the figure. All three profiles are plotted in a reduced scale (*i.e.* the peak height is normalized to unity) so that their maxima coincide.

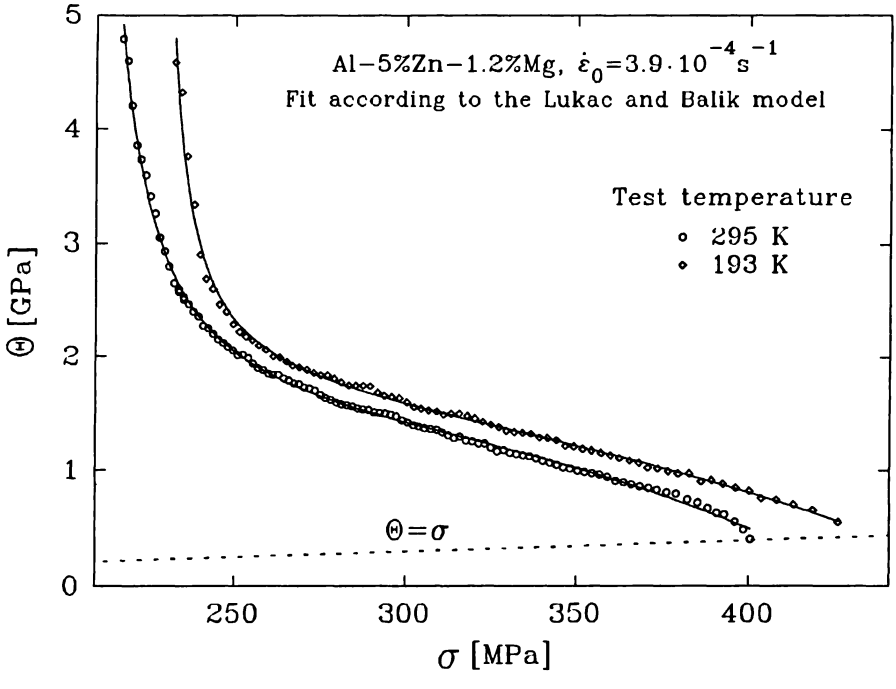

Fig. 15
Result of fitting the Lukáč and Balík model for Al–5%Zn–1.2%Mg alloy deformed at the initial strain rate $\dot{\varepsilon}_0 = 3.9 \times 10^{-4}\,s^{-1}$ at two different temperatures.

For the evaluation of peak profiles a program developed by Borbély and Ungár was used [56]. The values of dislocation densities are given in table 3 for i) the initial states (after annealing) of both Al–Mg alloys, ii) samples of both Al–Mg alloys deformed to fracture at various temperatures and iii) samples of Al–2.6%Mg alloy deformed to four various plastic strains at room temperature.

We can see a good correspondence of the values obtained for the initial states of both alloys in the two sets of measurements where different diffraction vectors were used ($\vec{g} = [200]$ and $\vec{g} = [220]$, respectively). For an illustration — the dislocation density obtained for an (underformed) aluminium monocrystal was $\varrho = (5.3 \pm 1.2) \times 10^{13}\,m^{-2}$. The value is very close to the values obtained for the initial states of both Al–4.8%Mg and Al–2.6%Mg alloys, from which we may assume that the effect of foreign atoms on the values of dislocation densities obtained by the method (XPA) can be neglected. In a perfect silicon crystal, the

dislocation density was found to be $\varrho = (1.9 \pm 0.7) \times 10^{13}\ m^{-2}$. This value is too high to represent the real dislocation density and can be taken as a treshold level (*i.e.* 'zero' offset) of the method.

Alloy	T_d [K]	$\dot{\varepsilon}_0$ [s^{-1}]	ε [%]	$\vec{g}$	ϱ [m^{-2}]	*Remark*
Al–2.6%Mg	–	–	–	[200]	$(5.7 \pm 1.2) \times 10^{13}$	*Initial state*
	295	3.4×10^{-4}	0.70	[200]	$(1.12 \pm 0.09) \times 10^{14}$	*Experiment stopped*
	295	3.4×10^{-4}	2.75	[200]	$(3.0 \pm 0.4) \times 10^{14}$	*Experiment stopped*
	295	3.4×10^{-4}	11.0	[200]	$(9.0 \pm 0.7) \times 10^{14}$	*Experiment stopped*
	295	3.4×10^{-4}	22.0	[200]	$(1.14 \pm 0.08) \times 10^{15}$	*Till fracture*
	295	3.4×10^{-4}	21.1	[220]	$(1.18 \pm 0.09) \times 10^{15}$	*Till fracture*
	473	3.4×10^{-4}	21.4	[220]	$(5.1 \pm 0.4) \times 10^{14}$	*Till fracture*
Al–4.8%Mg	–	–	–	[220]	$(4 \pm 1) \times 10^{13}$	*Initial state*
	295	4.3×10^{-4}	26.3	[220]	$(1.8 \pm 0.1) \times 10^{14}$	*Till fracture*
	423	4.3×10^{-4}	39.5	[220]	$(5.8 \pm 0.9) \times 10^{14}$	*Till fracture*
	523	4.3×10^{-4}	29.8	[220]	$(2.7 \pm 0.5) \times 10^{14}$	*Till fracture*

Table 3

Average dislocation density, as determined by means of XPA, of the samples of Al–4.8%Mg and Al–2.6%Mg alloys, deformed at various conditions.

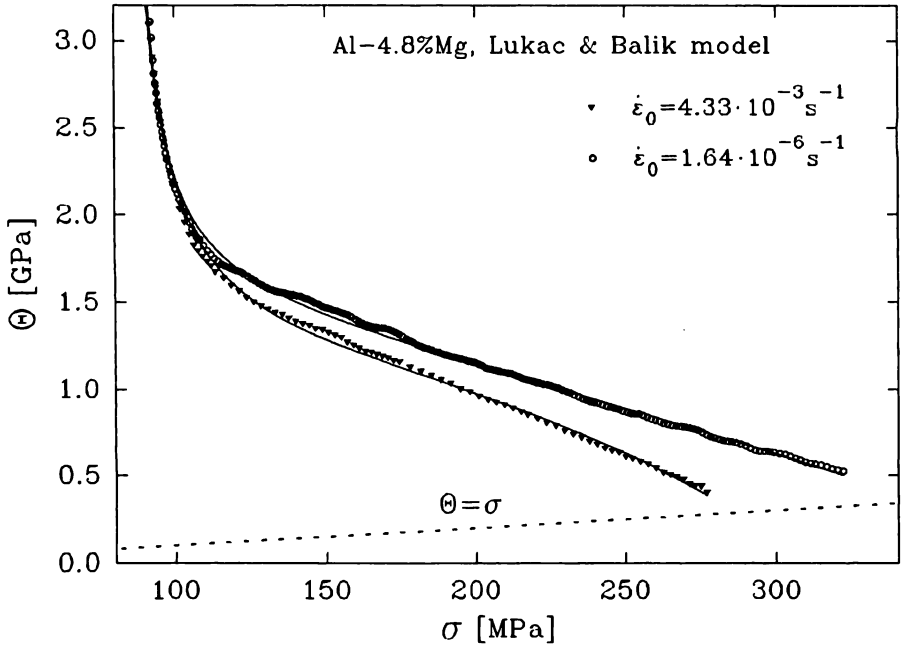

Fig. 16

Result of fitting the Lukáč and Balík model for Al–4.8%Mg alloy deformed two different strain rates at room temperature.

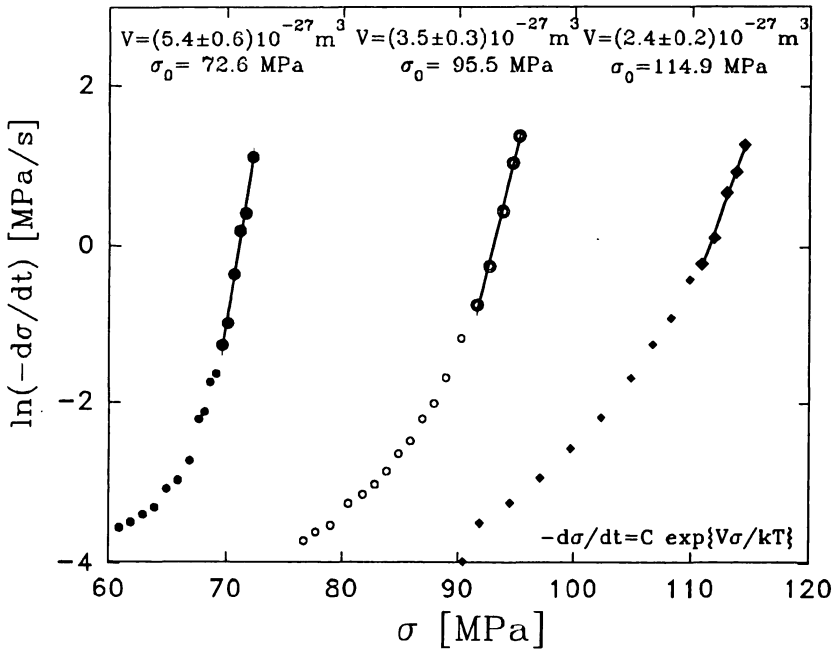

Fig. 17
Logaritmic plot of the stress dependence of the rate of stress decrease on the beginning of stress relaxations in Al–2.6%Mg alloy tested at 423 K.

5. Discussion

5.1 Work Hardening

In this section we will separately discuss the values of the parameters of work hardening models of Malygin [8] and Lukáč and Balík [9], as obtained from the fit procedure, and put them into connection with the values predicted by theory, observed microstructure (from TEM) and measured dislocation density (by means of XPA).

5.1.1 Yield Stress

The values of the yield stress σ_y determined in both fits are almost equal and, for both Al–Mg alloys, at the same time also appreciably lower than the experimental values of σ_{02} (the flow stress at 0.2% offset strain). In most cases $\sigma_y \approx \sigma_{01}$ holds. This is in accordance with the results of Lukáč and Balík [9] who found the ratio σ_{02}/σ_y to be between 1.1 and 1.2 for Cu–9 wt.%Ni alloy deformed at various temperatures ranging from room temperature up to 573 K. For the Al–5%Zn–1.2%Mg alloy are, in contrary, the values of the fitted yield stress σ_y roughly equal to the experimental σ_{02} values.

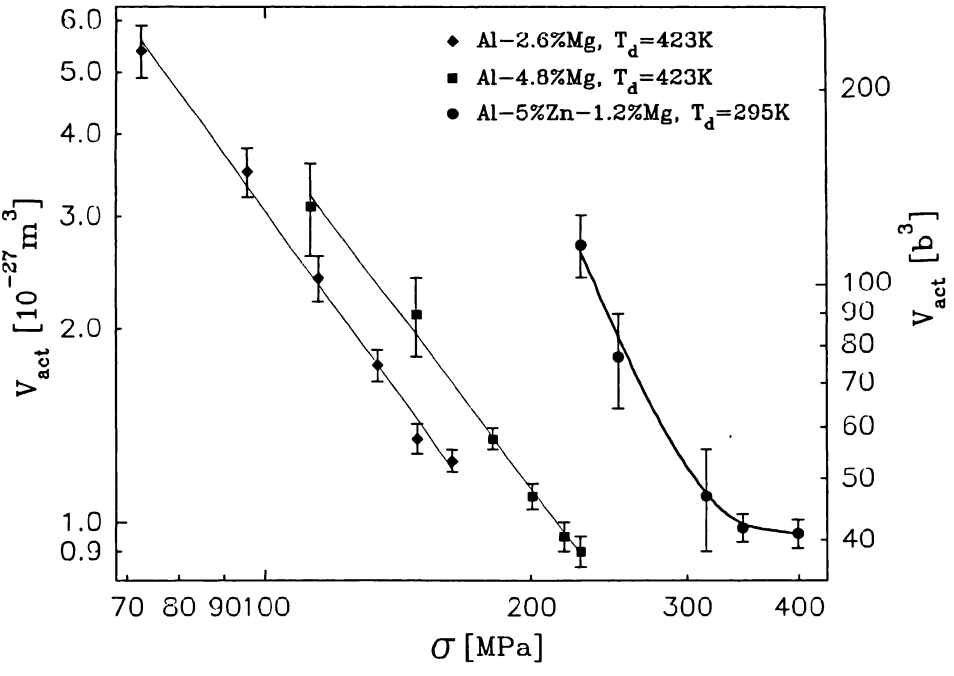

Fig. 18
Bilogaritmic representation of the stress dependence of the activation volume for the three alloys.

5.1.2 The Parameter $\mathscr{A}$

In both models [8, 9], the $\mathscr{A}$ parameter, which is connected with the non-dislocation obstacles, should increase with the increasing strain rate but should not depend on temperature. The increase of the $\mathscr{A}$ parameter with strain rate was observed in both models at room temperature. The invariance with temperature seems to be fulfilled for both Al–Mg alloys in the temperature range up to about 400 K = $0.43T_m$ only. This is exactly the temperature where a change in the character of deformation (an upward curvature in the temperature dependence of annihilation parameter $\mathscr{C}$) was observed by Malygin [8] in pure (4N5) aluminium. In both models for the mean particle spacing holds

$$L_p = \frac{1}{2} M^3(\alpha G)^2 b\mathscr{A}^{-1} \tag{40}$$

where $\alpha \approx 0.5$ is a multiplication factor [8] and $b = 2.86 \times 10^{-10}$ m is the Burgers vector [57]. If we take the room temperature values $\mathscr{A} = (9 \pm 1) \times 10^{15}$ Pa^2 for Al–4.8%Mg, $\mathscr{A} = (11 \pm 1) \times 10^{15}$ Pa^2 for Al–2.6%Mg and $\mathscr{A} = (20 \pm 5) \times 10^{15}$ Pa^2 for Al–5%Zn–1.2%Mg we obtain (for $G = 26.5$ GPa [57]) the mean particle spacing $L_p = (77 \pm 8)$ μm, $L_p = (63 \pm 8)$ μm and $L_p = (35 \pm 9)$ μm, respectively. These

values are in good accordance with the mean grain size values, which were determined to be (85 ± 9) μm, (66 ± 4) μm and (22 ± 7) μm, respectively. This together with the observation of the microstructure (only very few precipitates were observed on TEM micrographs of Al–4.8%Mg alloy, whereas no precipitates were observed in Al–2.6%Mg alloy) lets us assume that the increase of $\mathscr{A}$ for temperatures above 400 K can be attributed to the formation of subgrain boundaries [58, 59, 60].

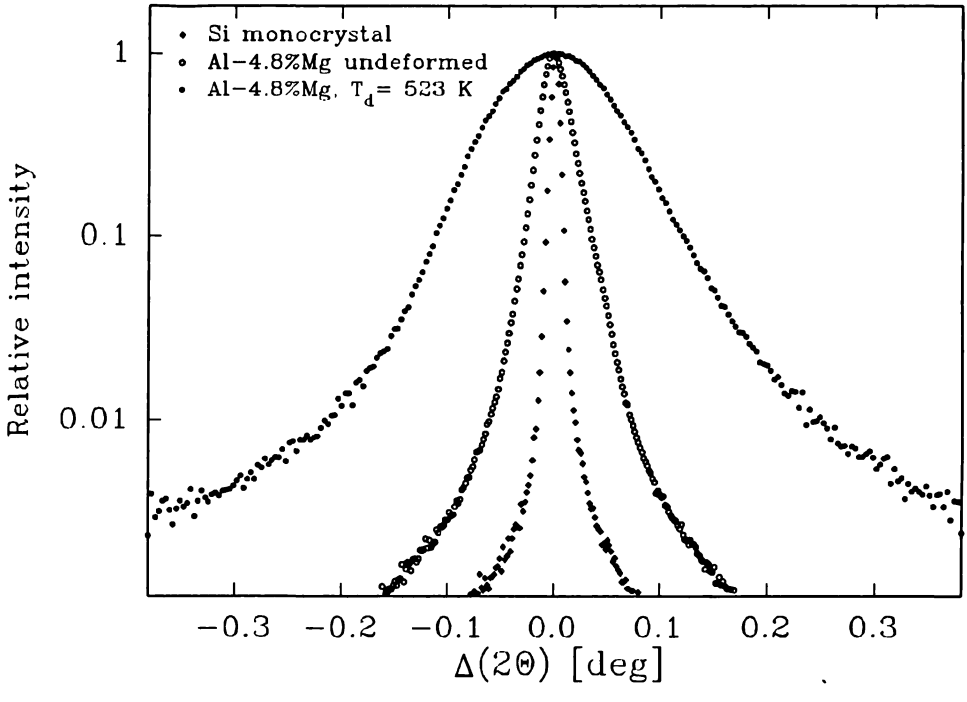

Fig. 19
Logaritmic plots of typical peak profiles obtained for Al–4.8%Mg alloy in i) initial state and ii) after deformation to fracture at 523 K (ε_{tot} = 29.8%).

5.1.3 The Parameter $\mathscr{B}$

The $\mathscr{B}$ parameter relates to the work hardening due to the interaction with forest dislocations. It should not depend on temperature and also the strain rate dependence should be very moderate. The first condition is fulfilled for the test temperatures lower than 400 K, similarly as by the $\mathscr{A}$ parameter. No effect of strain rate was observed (*i.e.* no significant changes of the values of fit parameters). In the Malygin model holds $b\kappa_f = 2\mathscr{B}/M^2\alpha G$. From the value $\mathscr{B} \approx 1.5$ GPa which was found by the second set of the Al–4.8%Mg alloy, we get $b\kappa_f = 2.4 \times 10^{-2}$. By other sample sets the results are similar. Malygin [8] obtained for pure aluminium $b\kappa_f$ equal to (1 to 2) $\times 10^{-2}$. The agreement is satisfactory.

In the Lukáč and Balík model [9] the slip length of dislocations is given as [3, 6]

$$L = \frac{1}{\sqrt{\varrho}} \frac{M^2 \alpha G}{2\mathscr{B}} . \tag{41}$$

If we take again the room temperature values for the second set of the Al–4.8%Mg alloy, $\mathscr{B} = (1.3 \pm 0.2)$ GPa and the dislocation density $\varrho = (1.8 \pm 0.1) \times 10^{15}\ \mathrm{m}^{-2}$ (see §4.1.4) we get $L = (1.3 \pm 0.2)$ μm. Similarly, from the room temnperature value for the Al–2.6%Mg alloy, $\mathscr{B} = (1.4 \pm 0.2)$ GPa and the dislocation density $\varrho = (1.18 \pm 0.09) \times 10^{15}\ \mathrm{m}^{-2}$ we get $L = (1.3 \pm 0.3)$ μm. The computed values of dislocation slip length correspond to microstructural observations: Dislocation bands with the distance of ≈ 1.5 μm and cell structure with cell size about $2 \times 8\ \mu\mathrm{m}^2$ were observed in Al–4.8%Mg and Al–2.6%Mg alloys at room temperature, respectively. (Lamellar structures formed by elongated cells were observed by many authors [61, 62, 63, 64] and termed 'lamellar boundaries' by Hughes and Hansen [64].) The slip length can be thus correlated with the cell size or periodicity of the lamellar structure.

At this place we will further check the consistency of our approach (*i.e.* the conception of the models [8, 9]) by comparing the values of the activation volume (see figure 18) with the measured dislocation density as given in §4.1.4: If we assume the activation volume in the form

$$V_{\mathrm{act}} = lbd\,, \tag{42}$$

where l is distance of the obstacles to dislocation motion, d is their width and b is Burgers vector, and take $d \approx 2b$ for forest dislocations (see *e.g.* [13, 65]) and $l = 1/\varrho^{1/2}$, we obtain in the case of the Al–4.8%Mg alloy for the dislocation density $\varrho = (1.8 \pm 0.1) \times 10^{15}\ \mathrm{m}^{-2}$ the value of the activation volume $V_{\mathrm{act}} = (3.8 \pm 0.5) \times 10^{-27}\ \mathrm{m}^3$. This value is slightly higher than the value of the activation volume obtained from stress relaxations (see §4.1.3) which varies from 1 to $3 \times 10^{-27}\ \mathrm{m}^3$. The accordance is satisfactory if we realize the approximation of the obstacle width $(d \approx 2b)$ and the fact that the distribution of dislocations is in fact inhomogeneous [54]. We can conclude that the activation volume is most probably connected with the intersection of forest dislocations and forest dislocations present thus the main obstacles for mobile dislocations.

5.1.4 The Parameter $\mathscr{C}$

The $\mathscr{C}$ parameter relates to recovery due to cross-slip and increases (with the exception of the highest test temperature by the Al–2.6%Mg alloy) in both models with increasing temperature, as can be expected due to the thermally activated character of cross-slip. The lower values for the highest deformation temperatures can be attributed to an onset of another recovery process which changes severely the character of the work hardening curve: The massive effect of recrystallization may become crucial and suppress the other, more subtle, processes as cross-slip

and/or climb of dislocations. This is probably the case of the highest test temperature for the Al–2.6%Mg alloy. The $\mathscr{C}$ parameter should decrease with increasing strain rate due to the thermally activated character of cross-slip. However, for both Al–Mg alloys, such a dependence was observed only for the values obtained from the Lukáč and Balík model. In the Malygin model the dependence is inverse. However, the relative changes are very small. For the annihilation parameter κ_a in the Malygin model holds equation [8]

$$\kappa_a = \frac{\omega_s^{5/2} G}{24\pi^2 \alpha \tau_c}, \tag{43}$$

where $\omega_s \approx 0.5$ [8] is the share of screw segments on the expanding dislocation loops. For the yield stress 43 MPa relation (43) gives $\kappa_a = 3 \pm 1$, whereas for the fit value $\mathscr{C} = 8 \pm 1$ we, according to equation (8), get $\kappa_a = 5 \pm 1$. This difference is comparably high, nevertheless we must realize all the approximations made (e.g. the idealized values $\omega_s = 0.5$ and $\alpha = 0.4$ were taken) in the model of Malygin [8].

5.1.5 The Parameter $\mathscr{D}$

For the Al–Mg alloys, the mean values of the $\mathscr{D}$ parameter in the Lukáč and Balík model were found to be negative for the temperatures above room temperature which is in contradiction to the theory.On the other hand, at higher temperatures, the standard deviation of the $\mathscr{D}$ parameter value is in all cases comparable to the mean value of $\mathscr{D}$. We can therefore conclude that the $\mathscr{D}$ parameter is, in the case of higher temperatures, not significant for the quality of the fit. This conclusion is not very surprising – the effect of dynamic recrystallization at the temperatures higher than about 400 K is obvious from the wavy form of stress-strain curves in both alloys. (The models [8, 9] are not designed for the regions where dynamic recrystalization occurs and are there thus not applicable.) The limit of $\approx$400 K is in accordance with the conclusions of sections §5.1.2 and §5.1.3.

The fact that the quality of the fit (*i.e.* Q parameter) is not significantly better for the Lukáč and Balík model (at temperatures below $\approx$400 K), is in contradiction to the resuts obtained by Lukáč and Balík for Cu–9wt.%Ni alloy [9] where the $\mathscr{D}$ parameter was found to be significat and positive in all cases and the quality of the fit was much better for the Lukáč and Balík model [9] than for the Malygin model [8]. We assume this difference to be caused by the fact that cross-slip in the Al–4.8%Mg alloys is much easier as compared to the above mentioned alloys as a result of a different structure of these alloys.

We should realize three following facts: i) Precipitates and GP zones were observed in the Cu–9wt.%Ni alloy in [9] and in the Al–5%Zn–1.2%Mg alloy in the present case, whereas no particles were observed in the Al–4.8%Mg and Al–2.6%Mg alloys; ii) Similarly, both the Al–4.8%Mg and the Al–2.6%Mg alloy

exhibit the PLC effect whereas the Cu–9wt.%Ni and the Al–5%Zn–1.2%Mg alloy in aged state (*i.e.* in the state used for the evaluation of work hardening) not, which is also an evidence of different mechanisms of plastic deformation in respective cases; iii) The less favorable conditions for cross-slip in the Cu–9wt.%Ni alloy as compared with the Al–4.8%Mg and Al–2.6%Mg alloys follow directly from the lower stacking fault energy (and consequently also higher distance between partial dislocations) in Cu. The effect of climb, in Al–4.8%Mg and Al–2.6%Mg alloys, can be then (due to easy cross-slip) diminished or climb possibly does not manifest (macroscopically) at all. At higher temperatures recrystallization comes into operation, too. In such a case, climb of dislocations is not crucial for the dynamic recovery, and does not affect the shape of the work hardening curve.

The $\mathscr{D}$ parameter should, according to (11) increase with decreasing strain rate. However, it can be seen [53, 54] that the observed strain rate dependence (see $\mathscr{D}$ parameter values for Al–4.8%Mg alloy at room temperature) is just inverse. The consequence of this fact is obvious from figure 16: The $\Theta(\sigma)$ curve for the initial strain rate $\dot{\varepsilon}_0 = 4.3 \times 10^{-3}\,\mathrm{s}^{-1}$ lies below the curve corresponding to $\dot{\varepsilon} = 1.6 \times 10^{-6}\,\mathrm{s}^{-1}$ and, in addition to this, also the downward curvature is higher at higher stresses for $\dot{\varepsilon}_0 = 4.3 \times 10^{-3}\,\mathrm{s}^{-1}$. Similar effect of strain rate on dynamic recovery was observed by Balík and Lukáč [30] for Al–3.3%Mg alloy at room temperature and was attributed to the fact that dynamic strain ageing impedes dynamic recovery all the more as the strain rate is decreased.

The quality of the fit Q for Al–5%Zn–1.2%Mg alloy is in all cases significantly better in favour of the Lukáč and Balík model. In addition to this, the $\mathscr{D}$ parameter is here in all cases positive and the relative mistake is small by the second set of samples (*i.e.* the parameter is in this case significant for the fit). Since in the Al–5%Zn–1.2%Mg alloy also some evidence of stage IV (re-hardening) of work hardening was observed (for the details and definitions on late stages of deformation see *e.g.* [58, 66]), which is not the case by the both Al–Mg alloys (Compare also the stress dependences of the activation volume for respective cases in figure 18: We assume that the deviating behaviour of the activation volume for higher stresses in the case of the Al–5%Zn–1.2%Mg alloy indicates the onset of stage IV hardening.) we may conclude, that the Lukáč and Balík model is also successful in description of later stages (IV, eventually V) of work hardening.

5.1.6 Evolution of dislocation density

The strain dependence of the average dislocation density, as measured by means of XPA (given in table 3 in §4.1.4) presents another possibility to perform a check of the model concepts independently of the work hardening behaviour (*i.e.* tensile tests) by comparing the experimental data with the evolution equation for the dislocation density which is, in the Malygin model [8], given by equation (6).

$$\frac{\partial \varrho}{\partial \gamma} = \kappa_{\mathrm{m}} + \kappa_{\mathrm{f}} \varrho^{1/2} - \kappa_{\mathrm{a}} \varrho \,.$$

The values $\partial\varrho/\partial\gamma$ can be in the first approximation determined from the ratio of increments in ϱ and ε between two following rows in table 3. (Due to very small amount of measurements, this seems to us to be the only applicable method.)

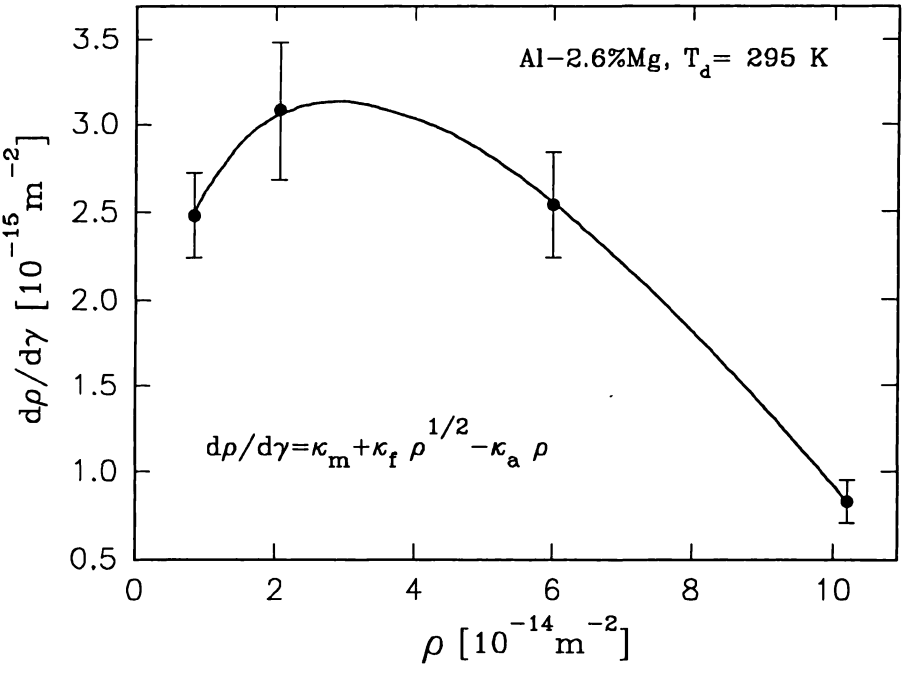

Fig. 20

The plot of $\partial\varrho/\partial\gamma$ against ϱ for the Al–2.6%Mg alloy deformed to various plastic strains at room temperature.

The resulting plot of $\partial\varrho/\partial\gamma$ against the average dislocation density ϱ is given in figure 20 together with a fit according to equation (6). The values of the parameters obtained from the fit were determined to be $\kappa_m = (1 \pm 1) \times 10^{14}\,m^{-2}$, $\kappa_f = (3 \pm 1) \times 10^{8}\,m^{-1}$ and $\kappa_a = 7 \pm 3$. (The errors of the values are standard deviations obtained from the least square fit and present thus only the lowest estimate.) We can compare these values with the results of fits of the work hardening curves (*i.e.* hardening models [8, 9]): From the value $\mathscr{A} = (1.0 \pm 0.2) \times 10^{16}\,Pa^2$ obtained from the fit of the Malygin model [8], we obtain $\kappa_m = (5 \pm 1) \times 10^{13}\,m^{-2}$. The agreement is satisfactory. The value of κ_f corresponds to $b\kappa_f \approx 8 \times 10^{-2}$ which is rather high (see §5.1.3). Similarly the value of κ_a yields, according to equation (8), $\mathscr{C} = 11 \pm 5$ which is twice as much as the value of $\mathscr{C} \approx 6$ obtained from the work hardening curves.

These differences, together with the high errors of the fit parameters (κ_m, κ_f and κ_a) can be attributed to the fact that the number of points in the $\partial\varrho/\partial\gamma$ *vs.*

ϱ dependence is very low (and the fit is thus overparametrized). A solution seems to be obvious — to decrease the deformation step between the samples in order to obtain more points in the dependence and a better quality of the fit. However, it seems that the present material (*i.e.* Al–2.6%Mg alloy) is rather unsuitable for XPA measurements due to its relatively small grain size. The small grain size results in difficulties with precluding (simultaneous) reflexes from two grains and also with achieving reasonably high intensities (and reasonable short measuring times). The accuracy of the measurement is thus not high enough and decreasing the deformation step is of no use. Experiments with some coarse-grained materials are desirable.

5.2 PLC effect

5.2.1 Numerical checks

In the following we will restrict ourselves to the analysis of the strain rate dependence of the critical strain of the Al–4.8%Mg and Al–2.6%Mg alloys at room temperature. As has already been said above the Al–5%Zn–1.2%Mg alloy is not suitable for quantitative checks due to a massive effect of ageing at room temperature. We will confine to the low strain rate limit only, because it is not possible to detect the onset of jerky flow with sufficient accuracy on the high strain rate limit. This fact has been already reported by Balík and Lukáč [30]. The experimental low strain limit at room temperature was interpolated according to equation

$$y = \frac{ax^b}{\exp\{cx^e\} + d}, \tag{44}$$

where x is substituted for ε_c, y for $\dot{\varepsilon}_c$ and a to e are parameters. It should be stated clearly that the interpolation function (44) was chosen from a great number of possible functions only on the basis how good it follows the course of the experimental $\varepsilon_c(\log \dot{\varepsilon}_c)$ dependence and has thus no connection to the theory.

The true plastic strain was transformed into the shear strain according to relation $\gamma = M\varepsilon$, where $M = 3.06$ is the Taylor factor for f.c.c. metals. The data $\partial\dot{\gamma}_c/\partial\gamma$, $\partial^2\dot{\gamma}_c/\partial\gamma^2$ were fitted with equation (30) and the values of parameters κ_1, κ_3, C_2 and C_4 were found. For the fit a leastsquare iterative technique was used. Afterwards, $\dot{\varepsilon}_c$ was again computed numerically according to (30) for each point. The result of this procedure is presented in figure 21 for the Al–4.8%Mg alloy. The parameter values were found to be $\kappa_1 = (6 \pm 4) \times 10^{-10}\,\mathrm{s}^{-2}$, $\kappa_3 = (3 \pm 2) \times 10^{-5}\,\mathrm{s}^{-1}$, $C_2 = 14 \pm 3$ and $C_4 = 32 \pm 5$ for the Al–4.8%Mg alloy. If we use equations derived by Balík and Lukáč [30]

$$\dot{\gamma}_{cs} = [(\kappa_1 C_4)^{1/2} - \kappa_3]/C_2 \tag{45}$$

$$\varrho_{ms}/\varrho_s = (C_4/C_2)\,[(\kappa_1 C_4)^{1/2} - \kappa_3]/(\kappa_1 C_4)^{1/2} \tag{46}$$

we can, in the saturation limit, obtain the critical strain rate $\dot{\gamma}_{cs} = (5 \pm 2) \times 10^{-6}\,\mathrm{s}^{-1}$ and the ratio of the mobile and forest dislocation densities $\varrho_{ms}/\varrho_{fs} = 1.3 \pm 0.6$. The

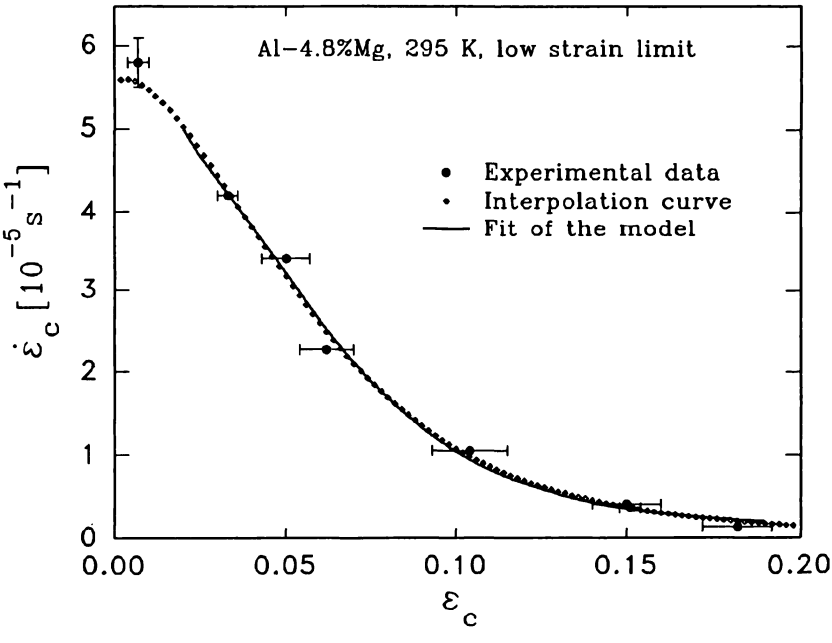

Fig. 21
Low strain limit of Al–4.8%Mg at room temperature: experimental data, interpolation and fit.

former value correponds to $\dot{\varepsilon}_{cs} = (1.6 \pm 0.6) \times 10^{-6}\,s^{-1}$ which seems to be in a good agreement with our experimental results. The latter value is close to the value ≈ 1.2 which follows from the numerical calculations of Kubin and Estrin [28].

For the Al–2.6%Mg alloy the fit gives following parameter values: $\kappa_1 = (1.0 \pm 0.5) \times 10^{-8}\,s^{-2}$, $\kappa_3 = (6 \pm 3) \times 10^{-4}\,s^{-1}$, $C_2 = 90 \pm 30$ and $C_4 = 55 \pm 20$, from which, according to equations (45) and (46) follows $\dot{\varepsilon}_{cs} = (8 \pm 3) \times 10^{-7}\,s^{-1}$ and $\varrho_{ms}/\varrho_{fs} = 0.08 \pm 0.04$. The latter value seems to be rather low, nevertheless, it is in good correspondence with the value $\varrho_{ms}/\varrho_{fs} = 0.036$ reported by Balík and Lukáč [30] for the Al–2.84%Mg alloy. This leads us to the conclusion that both in Al–2.6%Mg in the present case and in the Al–2.84%Mg alloy in [30] is either the density of forest dislocations high or the mobile dislocation density is low (or the both cases) as compared with the Al–4.8%Mg alloy.

It was possible to obtain all fit parameters with a good physical meaning from a "free" fit only for ε_c higher than about 2% in the case of Al–4.8%Mg alloy and about 0.8% in the case of Al–2.6%Mg alloy. The fits for $\varepsilon_c \leq 2\%$ for the Al–4.8%Mg alloy and $\varepsilon_c \leq 0.8\%$ for the Al–2.6%Mg alloy did not yield acceptable values of fit parameters. There are two possible explanations: (a) As has been already mentioned by Balík and Lukáč [30], the elementary incremental strain Ω as given by the equation (22) supposes the forest dislocations to be the only obstacle for the mobile dislocation. Nevertheless, it is just the first approximation: More

generally, it is necessary to take into account other possible locking points of non-dislocational origin. In addition to this, in a detailed analysis it would be necessary to discuss also the processes connected directly with dynamic strain ageing, as for instance locking of dislocations by the foreign atoms, which can also affect the waiting time [30] and lead to a more complex form of the equation (22). However, this is not the aim of this work. (b) The equations (23) and (24) are not suitable for the description of the evolution of dislocation densities in the present case. In such a case a modification of these equations should be found which is in accordance with the known work hardening behaviour of the investigated alloy. In the following we will discuss this two possibilities in more detail.

5.2.2 Elementary incremental strain

The influence of the average spacing between the foreign atoms on the elementary strain has been discussed recently by Kalk *et al.* [67]. In such a case the effective average free slip distance L_0 is lower than the average distance of forest dislocations $L_f = \varrho_f^{-1/2}$, which corresponds to the situation when the forest dislocations form the only pinning points, and equation (22) has the form

$$\dot{\gamma} = b\varrho_m L_0(\varrho_f, c_{FA})/t_w = \Omega/t_w , \tag{47}$$

where c_{FA} is concentration of foreign atoms. In a good approximation [67] L_0 is given by $1/L_0 = 1/L_f + 1/L_{FA}$ where L_{FA} is the average spacing of glide obstacles formed by foreign atoms. The decrease in L_{FA} (*e.g.* by increasing the solute concentration c_{FA}) should lead to a decrease of Ω and, if we suppose t_w to be constant, also to a decrease of $\dot{\gamma}_c$.

However, if we compare the $\varepsilon_c(\log \dot{\varepsilon}_c)$ dependences obtained for the Al–4.8%Mg and Al–2.6%Mg alloys in the present case with the results for the Al–3%Mg alloy [30] we can see an opposite effect. Since the mechanical and thermal processing of the Al–4.8%Mg and Al–2.6%Mg alloys was exactly the same and the grain size difference between these two alloys is thus relatively small (91 μm and 66 μm, respectively), we suppose that it is possible to exclude the effects of grain size and thermal processing (solution treatment) as not crucial in this case. (This assumption is further supported by the fact that the values of the critical strains for Al–3%Mg alloy [30] and Al–2.6%Mg alloy differ from each other appreciably less than the values for both these alloys differ from the values for the Al–4.8%Mg, although the difference in the grain size between the Al–3%Mg alloy and Al–2.6%Mg alloy is relatively big — 18 μm and 66 μm, respectively). Hence we can finally conclude that the observed differences in the $\varepsilon_c(\log \dot{\varepsilon}_c)$ dependences for respective alloys are not consistent with the mechanism proposed by Kalk *et al.* [67] and the adoption of equation (1) in the sence of equation (47) is thus not necessary.

Another possible mechanism which should be taken into account is pinning by "stable" particles (precipitates). The effect of particles on the critical strain in Al alloys has been recently investigated by Chan *et al.* [68] who showed that the

critical strain decreases with the decreasing particle spacing L_p. It is not easy to make a quantitative comparison of the pinning effects of the forest dislocations and particles but it can be assumed that some effect of particles is to be expected if the mean particle spacing in the matrix L_p is comparable or lower than the mean spacing of forest dislocation $L_f = \varrho_f^{-1/2}$. In such a case, the equation (22) will have the following form

$$\dot{\gamma} = b\varrho_m \mathscr{F}(\varrho_f, L_p)/t_w = \Omega/t_w\,, \tag{48}$$

where, like in equation (47), $\mathscr{F}$ is some function of ϱ_f and L_p. The attempt to obtain the mean dislocation spacing directly from the observations of microstructure by TEM showed itself to be problematic because of a very small amount of particles present in the matrix which were observed only accidentaly on some foils. Therefore, we will make an estimate based on the known hardening behaviour.

In the previous section §5.1 we have shown that the stress dependence of the work hardening coefficient Θ defined by equation (1) can be satisfactory described by the models of Malygin [8] and of Lukáč and Balík [9]. From the analysis of the value of the model parameters made in §5.1 it follows that the distance of impenetrable obstacles (*i.e.* particles or precipitates) for dislocation motion can be put into connection with the mean grain size of the samples. The mean grain size in the present case is about 90 μm in the case of Al–4.8%Mg alloy and about 70 μm in the case of Al–2.6%Mg alloy. These values are much higher than the average dislocation spacing L_f, which is to be expected: If we take the initial value of the density of forest dislocations (on the beginning of plastic deformation) to be $\varrho_f \approx 10^{11}\,\mathrm{m}^{-2}$ (as follows from the results of X-ray Peak Profile Analysis measurements in §4.1.4 this value is low enough to represent the initial state – see also [28]), we obtain $L_f \approx 3$ μm. We can, therefore, in the present case, exclude the interaction of dislocation with non-dislocation obstacles as a mechanism which could lead to a modification of equation (1).

However, it should be pointed out that no plastic instabilities were observed in the very beginning of plastic deformation in the present case, whereas the effect of particles would manifestate mainly at very low strains, where the dislocation density is still relatively low as compared with the particle density (which remains constant). The presence of particles would result in the decrease of the critical strain [68].

5.2.3 Evolution of dislocation densities

In the search for a modified form of the evolution equations for the densities of mobile ϱ_m and immobile dislocations ϱ_f we will compare the equations (23) and (24) used by Kubin and Estrin [27] with the evolution equations used in the models of work hardening proposed by Malygin [8] and Lukáč and Balík [9]: Malygin [8] used the following set of equations:

$$\frac{\partial \varrho_m}{\partial \gamma} = K_m/b^2 - K_i/b^2 - K_a\varrho + (K_f/b)\,\varrho^{1/2} \tag{49}$$

$$\frac{\partial \varrho_i}{\partial \gamma} = K_i/b^2\,,\ \varrho = \varrho_m + \varrho_i \tag{50}$$

where K_x (x = m, i, a, f) are parameters (for definitions see §2.1.1). Here the density of immobile dislocations was denoted ϱ_i to distinguish from ϱ_f in the model of Kubin and Estrin [27] since the definitions are different. Lukáč and Balík take into account another recovery mechanisms in addition to cross-slip: At the medium temperature range climb of edge dislocations will play role [9]. In such case an additional term $-\ K_c b^2 \varrho^{3/2}$ appears in the equation (49), where K_c is a model parameter which relates to climb.

Adding equations (23) and (24) gives

$$\partial \varrho/\partial \gamma = C_1/b^2 - C_4 \varrho_f\,. \tag{51}$$

whereas from equations (49) and (50) follows

$$\frac{\partial \varrho}{\partial \gamma} = K_m/b^2 - K_a \varrho + \left(K_f/b\right) \varrho^{1/2} \tag{52}$$

Equation (51) is a modification of the evolution equation used by Estrin and Mecking [4] in their model of work hardening. However, we have shows in our previous works [18, 20] (concerned with work hardening in zirconium- and aluminium-based alloys) that the model of Estrin and Mecking is not able to describe the course of the whole $\Theta(\sigma)$ curve in any of the tested alloys. On the other side, the Malygin model [8] and the Lukáč and Balík model [9] have prooved themselve to be more realistic (see §4.1.2). Therefore we suppose that a modification of the equations (23) and (24) in the sense of equations (49) and (50) (or the adoption of (49) and (50) as has been made by Lukáč and Balík [9]) is necessary. This modification should lead at the same time to applicable models of both work hardening and plastic instabilities.

The following facts speak also for the conclusions made above: (a) Similarly as in the model of work hardening of Estrin and Mecking [4] it is not possible to fit the whole $\dot{\varepsilon}_c(\varepsilon)$ dependence in the model of Kubin and Estrin [27, 28]. (b) The strain dependence of the elementary incremental strain Ω that was observed in the present work (note that the dependences $\Omega(\varepsilon)$ and $\dot{\varepsilon}_c(\varepsilon)$ are same [27, 30]) does not correspond to the dependences obtained by Kubin and Estrin from computer simulations based on equations (23) and (24).

6. Conclusions

Deformation behaviour of two pure aluminium–magnesium alloys with weight concentrations of 2.6% Mg and 4.8% Mg, respectively, and a commercial aluminium alloy of type 7020 with 5 wt.%Zn and 1.2 wt.%Mg has been

investigated in the temperature range 193 – 523 K. Tensile tests were performed at constant but various cross-head speeds giving initial strain rates from the interval $4.76 \times 10^{-6}\,s^{-1} \leq \dot{\varepsilon}_0 \leq 2.38 \times 10^{-2}\,s^{-1}$. Work hardening curves are analyzed and compared with the predictions of the models proposed by Gottstein and Argon [6], Prinz and Argon [7], Malygin [8], and Lukáč and Balík [9]:

- Only singular and stage II hardening as well as glide recovery by cross-slip (stage III) are involved in the case of Al–4.8%Mg and Al–2.6%Mg alloys, wherekas in the case of Al–5%Zn–1.2%Mg alloy also some evidence of stage IV (re-hardening) of work hardening curve was observed.
- Both the Malygin model [8] and the Lukáč and Balík model [9] are applicable at all strain rates in the whole temperature range, with exception of the highest test temperatures where a massive dynamic recrystallization takes place. The course of the work hardening curve is described satisfactory. The other two tested models suggested by Gottstein and Argon [6] and Prinz and Argon [7] yield a much worse description of the experimental work hardening curves.
- From the results of fitting of the Lukáč and Balík model follows that the recovery mechanism connected with climb of dislocations plays a minor role in Al–4.8%Mg and Al–2.6%Mg alloys deformed at higher temperatures, probably due to easy cross-slip. At lower temperatures the Lukáč and Balík model yields a more precise description of the deformation processes than the Malygin model. The Lukáč and Balík model is significantly better than the Malygin model for description of the deformation behaviour of Al–5% Zn–1.2%Mg alloy.
- The fit parameters correspond to the observed microstructure: The $\mathscr{A}$ parameter is related to the grain size. The slip length of dislocations, which can be derived from the $\mathscr{B}$ parameter, is related to the size of dislocation cells or the periodicity of dislocation band structure.

The critical strains for the onset and termination of PLC effect have been measured as a function of strain rate and temperature and compared with the model of Kubin and Estrin [27, 28]:

- The prediction of the model of Kubin and Estrin [27, 28] are found to be in a good qualitative agreement with the experimental data only for the strains higher than about 2% for Al–4.8%Mg alloy and about 0.8% for the Al–2.6%Mg alloy. Possible expanations of this fact are suggested.
- It seems that the influence of non-dislocation pinning of both solute and particle origin on the elementary incremental strain is not crucial in the present case. A modification of the equation for the elementary incremental strain thus seems not to be necessary.
- A modification of the evolution equations of the mobile and immobile dislocations used in the model of Kubin and Estrin is suggested, based on a known work hardening behaviour of the alloys.

Acknowledgements: The authors wish to thank Prof. Dr. W. Blum and Prof. Dr. Y. Brèchet for supplying the Al–4.8%Mg and Al–2.6%Mg alloys, respectively. Special thanks belong to Prof. Dr. E. Pink for supplying the machined samples of Al–5%Zn–1.2%Mg alloy. The assistance of Dr. M. Janeček and Ms. M. Čepová with the documentation of microstructure and of Prof. Dr. T. Ungár and Dr. A. Borbély with the evaluation of XPA measurements is gratefully appreciated. Thanks are also due to Ass. Prof. Dr. M. Zehetbauer who kindly granted the measuring time at the Siemens rotating Cu-anode generator at the Institute of Material Physics of the Vienna University. The second author is greately indebted to the Alexander von Humboldt Foundation for continued support. The work was supported by the Grant Agency of the Czech Republic under grant 106/96/0322 and the Grant Agency of Charles University under grants 154/1996 and 142/1996.

References

[1] Esmann, U. and Mughrabi, H., *Phil. Mag.* **A40**, 731 (1979).
[2] Taylor, G. I., *Proc. Roy. Soc.* **A145**, 362 (1934).
[3] Kocks, U. F., *J. Eng. Mater. Tech.* **98**, 76 (1976).
[4] Estrin, Y. and Mecking, H., *Acta metall.* **32**, 57 (1984).
[5] Roberts, W., *Processing and Structure* (Ed. G. Krausz) ASM, Metals Park, p. 109 (1984).
[6] Gottstein, G. and Argon, A. S., *Acta metall.* **35**, 1261 (1987).
[7] Prinz, F. and Argon, A. S., *Acta metall.* **32**, 1021 (1984).
[8] Malygin, G. A., *phys. stat. sol.* (a) **119**, 423 (1990).
[9] Lukáč, P. and Balík, J., *Key Eng. Mater.* **97–98**, 307 (1994).
[10] Zehetbauer, M., *Acta metall. mater.* **41**, 589 (1993).
[11] Zehetbauer, M. and Les, P., *Proc. 35th Ann. Conf. Metallurgists*, Metall. Soc. of CIM, p. 205 (Montreal, Canada, 1996).
[12] Nix, W. D., Gibeling, J. C. and Hughes, D. A., *Metal. Trans.* **A16**, 2215 (1985).
[13] Blum, W., Rosen, A., Cegielska, A. and Martin, J. L., *Acta metall.* **37**, 2439 (1989).
[14] Dobeš, F. and Blum, W., *phys. stat. sol.* (a) **144**, 343 (1994).
[15] Fang, X. F. and Dahl, W., *Mater. Sci. Eng.* **A203**, 36 (1995).
[16] Argon, A. S. and Haasen, P., *Acta metall. mater.* **41**, 3289 (1993).
[17] Trojanová, Z., Král, R. and Lukáč, P., *Proc. of EUROMAT '94*, p. 100 (Budapest H, 1994).
[18] Král, R., Trojanová, Z. and Lukáč, P., *Key Eng. Mate.* **97–98**, 359 (1995).
[19] Král, R., *MSc. Thesis*, Charles University, Prague (1992).
[20] Král, R., Lukáč, P. and Pink, E., *Key Eng. Mater.* **97–98**, 365 (1995).
[21] McCormick, P. G., *Acta metall.* **36**, 3061 (1988).
[22] Cottrell, A. H., *Phil. Mag.* **44**, 829 (1953).
[23] McCormick, P. G., *Acta metall.* **19**, 463 (1971).
[24] van den Beukel, A., *Acta metall.* **28**, 965 (1980).
[25] Balík, J. and Lukáč, P., *Czech J. Phys.* **B39**, 447 (1989).
[26] Mulford, R. A. and Kocks, U. F., *Acta metall.* **27**, 1125 (1979).
[27] Kubin, L. P. and Estrin, Y., *Acta metall. mater.* **38**, 697 (1990).
[28] Kubin, L. P. and Estrin, Y., *phys. stat. sol.* (b) **172**, 173 (1992).
[29] Kocks, U. F., Cook, R. E. and Mulford, R. A., *Acta metall.* **33**, 623 (1985).
[30] Balík, J. and Lukáč, P., *Acta metall. mater.* **41**, 1447 (1993).

[31] KUHLMANN-WILSDORF, D., in *Work Hardening* (edited by J. P. Hirth and J. Weertman), p. 97, Gordon & Breach, New York 1968.
[32] BILBY, B. A., COTTRELL, A. H., SMITH, E. and SWINDEN, K. H., *Proc. R. Soc. Lond.* **A279**, 1 (1964).
[33] ZAISER, G. and HÄNNER, P., *phys. stat. sol.* (b) **199**, 267 (1997).
[34] GOTTSTEIN, G. and KOCKS, U. F., *Acta metall.* **31**, 175 (1983).
[35] UNGÁR, T., MUGHRABI, H., RÖNNPAGEL, D. and WILKENS, M., *Acta metall.* **32**, 333 (1984).
[36] WILKENS, M. and ECKERT, H., *Z. Naturforschung* **19a**, 459 (1964).
[37] GROMA, I., UNGÁR, T. and WILKENS, M., *J. Appl. Cryst.* **21**, 47 (1988).
[38] UNGÁR, T., GROMA, I. and WILKENS, M., *J. Appl. Cryst.* **22**, 26 (1989).
[39] WILKENS, M., *phys. stat. sol. (a)* **2**, 359 (1970).
[40] WILKENS, M., *phys. stat. sol. (a)* **104**, K1 (1987).
[41] BORBÉLY, A., private communication (1996).
[42] BALÍK, J., JANEČEK, M. and LUKÁČ, P., *Mater. Sci. Eng.* **A159**, 143 (1992).
[43] CHMELÍK, F., TROJANOVÁ, Z., PŘEVOROVSKÝ, Z. and LUKÁČ, P., *Mater. Sci. Eng.* **A164**, 260 (1993).
[44] CHMELÍK, F., TROJANOVÁ, Z., LUKÁČ, P. and PŘEVOROVSKÝ, Z., *Acta Techn. ČSAV* **40**, 43 (1995).
[45] MUKAI, T., HIGASHI, K. and TANIMURA, S., *Mater. Sci. Eng.* **A176**, 181 (1994).
[46] PINK, E., *Acta metall.* **37**, 1773 (1989).
[47] RODRIGUEZ, F. and VENKADESAN, S., *Key Engn. Mater.* **103**, 257 (1995).
[48] PINK, E., WEBERNIG, W. M. and KRÓL, J., *Mater. Sci. Eng.* **93**, L1 (1987).
[49] PINK, E., private communication (1996).
[50] KUMAR, S., *Scripta metall. mater.* **33**, 81 (1995).
[51] NASH, J. E., *Compact Numerical Methods for Computers: Linear Algebra and Minimization*, Adam Hilger Ltd., Bristol 1979.
[52] CELÝ, J., *Programové moduly pro fyzikální výpočty*, Masaryk University, Brno 1985.
[53] KRÁL, R., *phys. stat. sol. (a)*, **157**, 255 (1996).
[54] KRÁL, R., LUKÁČ, P., ZEHETBAUER, M. and JANEČEK, M., *Acta Techn. ČSAV* **42**, 145 (1997).
[55] HAMERSKÝ, M., TROJANOVÁ, Z. and LUKÁČ, P., *Acta Techn. ČSAV* **37**, 263 (1992).
[56] BORBÉLY, A. and UNGÁR, T., private communication (1996).
[57] GRAY, D. E., *American Institute of Physics Handbook*, 3rd edition, p. II–62, McGraw-Hill, New York (1972).
[58] GIL SEVILLANO, J. and AERNOUDT, E., *Mater. Sci. Eng.* **86**, 35 (1987).
[59] WILKENS, M., UNGÁR, T. and MUGHRABI, H., *phys. stat. sol.* **104**, 157 (1987).
[60] KUHLMANN-WILSDORF, D. and HANSEN, N., *Scripta metall. mater.* **25**, 1557 (1991).
[61] UNGÁR, T., TÓTH, L. S., ILLY, J. and KOVÁCS, I., *Acta metall.* **34**, 1257 (1986).
[62] HOSFORD, W. F., *Trans. AIME* **230**, 12 (1964).
[63] LANGFORD, G. and COHEN, M., *Metall. Trans.* **6A**, 910 (1975).
[64] HUGHES, D. A. and HANSEN, N., *Metall. Trans.* **24A**, 2021 (1993).
[65] BLUM, W., PÖLLMANN, T., HOFFMAN, U. and WEIDINGER, P., *phys. stat. sol. (a)* **157**, 329 (1996).
[66] ZEHETBAUER, M. and SEUMER, V., *Acta metall. mater.* **41**, 577 (1993).
[67] KALK, A., NORTMANN, A. and SCHWINK, CH., *Phil. Mag. A* **72**, 1239 (1995).
[68] CHAN, K. S., CHEN, L. H. and LUI, T. S., *J. Mat. Sci.* **30**, 212 (1995).